

# POLITECNICO DI TORINO

Master's Degree in Mechanical Engineering

Master's Degree Thesis

## **Envelope-Based Rigid Ring Model of E-Scooter Tires: Development and Validation of Vertical Dynamics**



**Politecnico  
di Torino**

Supervisor

Prof. Alessandro Vigliani

Candidate

Mehanas Saleem

Co - Supervisor

Dr. Angelo Domenico Vella

## **Abstract**

In today's world, where the use of e-scooters as a convenient mode of transportation is on the rise, there is a need for study on their dynamics and handling. The aim of this thesis is to develop a matlab model able to compute key components of vertical dynamics involved in the motion of an e-scooter tyre going over small obstacles on the road. The obstacle enveloping behaviour of the tyre is of importance in order to accurately portray it's motion. Hence the first step undertaken is to develop in matlab, a program that allows one to input a given road profile and to obtain the effective road profile, using the MF SWIFT obstacle enveloping model.

To analyze the vertical dynamics of the tyre, it is suitable to use the MF SWIFT rigid ring model, for which the vertical belt stiffness, belt damping and residual stiffnesses need to be computed. The tyre of a Xiaomi pro II e-scooter is used for the experiments conducted to that end. Modal Analysis is conducted on a test set up of the tyre fitted with sensors, where the tyre is hammered at different points to excite the it's modes and analyze them using Simcenter Testlab. This yields information on the various modes of the tyre, where the radial mode is of interest for computation of the belt stiffness and damping.

The tyre is also subjected to a compression test where it is set up using a clamp to an MTS machine that delivers a load to the tyre quasi statically. The displacement of the tyre is recorded with respect to the applied load. From this experiment, one obtains the total radial stiffness of the tyre, from which the residual stiffness can be extracted. Footprint analysis is also conducted to correlate the contact patch length to vertical load.

Finally, the model is executed in Simulink and tested to obtain the vertical displacements, accelerations and forces exchanged, for various road profiles. The results obtained from the model are compared to experimentally obtained values for validation.

# Contents

Introduction .....	5
1. Literature Review .....	6
1.1 Enveloping models .....	6
1.1.1 The Development of Empirical Envelope Models.....	7
1.1.2 The Two Point Follower Model.....	8
1.1.3 Tandem Elliptical Cam Model .....	10
1.2 Dynamic Tyre Model .....	11
1.2.1 Multibody Models.....	11
1.2.2 Finite Element Models .....	12
1.2.3 Modal Models .....	12
1.2.4 Rigid Ring Model .....	13
2. MF Swift Model.....	14
2.1 Tandem Elliptical Cam Model .....	15
2.1.1 Cam Properties Evaluation.....	18
2.2 Rigid Ring Model .....	20
3. Experiments .....	23
3.1 Radial Stiffness Test .....	23
3.1.1 Post Processing and Results.....	24
3.2 Experimental Modal Analysis.....	29
3.2.1 Post Processing and Results.....	30
3.3 Footprint Analysis .....	34
4. Modelling .....	37
4.1 Envelope Model Results.....	37
4.1.1 Sensitivity Analysis .....	38
4.2 Simulink Model .....	42
4.2.1 Experiment and Results .....	43
<b>BIBLIOGRAPHY .....</b>	<b>46</b>

## List of Figures

Figure 1.1 Several Envelope Models Found in Literature .....	6
Figure 1.2. The rigid wheel response to a step obstacle.....	8
Figure 1.3 Comparison of Rigid Wheel and Quarter sine Basic Curves .....	9
Figure 1.4 Quarter sine basic curves for three different step heights .....	9
Figure 1.5 Basic Curve generated by elliptical cam.....	10
Figure 1.6 Comparison of elliptical and quarter sine basic curve.....	10
Figure 1.7. Different categories of Dynamic Tyre Models.....	11
Figure 1.8. Three-dimensional Multibody Tyre Model .....	11
Figure 2. 1 Magic Formula inputs and outputs .....	14
Figure 2. 2 Representation of Elliptical Cam Model generating effective road surface.....	15
Figure 2. 3 Diagram of 3-dimensional tandem elliptical cam model depicting cam arrangement .....	17
Figure 2. 4 Diagram of Tandem Model with loaded tyre indicating relation of paramters $R_0$ , $a$ and $b$ .....	18
Figure 2. 5 Comparison of outside contour of loaded tyre and Tandem model ellipse shape in zone of possible contact .....	19
Figure 2. 6 Result of the matlab code to fit the elliptical cam shape to tyre outside contour for a given unloaded tyre radius and footprint length .....	19
Figure 2. 7 The rigid ring model featuring the rigid ring, flexible sidewalls, the contact model which includes a small contact mass, slip model and residual stiffness and damping elements .....	20
Figure 2. 8 Simplified system to describe tyre vertical dynamics .....	20
Figure 2. 9 Three degree of freedom tyre vertical dynamics model .....	21
Figure 2. 10 Feedback cycle between enveloping model and rigid ring model that forms the basis for evaluating the vertical dynamics of the tyre .....	22
Figure 3. 1 Experimental setup of tyre on MTS machine for radial stiffness evaluation .....	23
Figure 3. 2 Plot of Raw Experimental Results .....	24
Figure 3. 3 Plot of Experimental data after deleting noise values and setting upper limit .....	25
Figure 3. 4 Comparison of experimental data with fitted curves of various polynomial orders at 30 bar inflation pressure .....	25
Figure 3. 5 Plot of three separate test results for Load vs displacement at 25 bar inflation pressure.....	25
Figure 3. 6 Plot of three separate test results for Load vs displacement at 35 bar inflation pressure.....	26

Figure 3. 7 Plot of three separate test results for Load vs displacement at 45 bar inflation pressure.....	26
Figure 3. 8 Plot of three separate test results for Load vs displacement at 40 bar inflation pressure.....	26
Figure 3. 9 Comparison of experimental data with fitted curves of various polynomial orders at 45 bar inflation pressure.....	27
Figure 3. 10 Comparison of experimental data with fitted curves of various polynomial orders at 25 bar inflation pressure.....	27
Figure 3. 11 Plot of Radial Stiffness as a function of vertical displacement for each inflation pressure.....	28
Figure 3. 12 Tyre setup for Experimental Modal Analysis.....	29
Figure 3. 13 Example of a stabilization diagram.....	30
Figure 3. 14 Second Modal Shape identified at 507.9 Hz.....	31
Figure 3. 15 First Modal Shape identified at 334.3 Hz.....	31
Figure 3. 16 Third Modal Shape Identified at 523.1 Hz.....	32
Figure 3. 17 Fourth Modal Shape identified at 608.3 Hz.....	32
Figure 3. 18 Fifth Modal shape identified at 610.4 Hz.....	33
Figure 3. 19 Plot of Residual Stiffness as a function of total vertical displacement at 35 bar inflation pressure.....	33
Figure 3. 20 Footprint captured of 35 bar pressure tyre at Loads of 1000 N and 500 N on Fujifilm prescale.....	34
Figure 3. 21 Plot of Contact patch dimensions measured at each Vertical Load input.....	35
Figure 3. 22 Plot of experimental results and corresponding fitted polynomial curve of contact footprint length vs Vertical load.....	36
Figure 4. 1 Effective road plot obtained using envelope model on a step obstacle of height 1 cm.....	37
Figure 4. 2 Effective road plot obtained using envelope model on a ramp obstacle of height 1 cm.....	37
Figure 4. 3 Effective road plot obtained from envelope model on a triangular obstacle of height 1 cm.....	38
Figure 4. 4 Depiction of piercing of Contact patch surface by obstacle when model has insufficient number of cams.....	38
Figure 4. 5 Comparison of envelope model results by varying the number of cams.....	39
Figure 4. 6 Zoomed in image of zone 1 in figure 4.5.....	39
Figure 4. 7 Zoomed in image of zone 2 in figure 4.5.....	40
Figure 4. 8 Comparison of envelope model results for varying number of cams while $l_s$ is increased by 2cm.....	40
Figure 4. 9 Comparison of envelope model results for varying number of cams while $l_s$ is increased by 2mm.....	40

Figure 4. 10 Plot of the test road profile used in experiments .....43  
Figure 4. 11 Comparison of experimental and model results of Rear wheel acceleration.....44  
Figure 4. 12 Comparison of experimental and model results of Rear wheel acceleration.....44

## List of Tables

Table 1 RMS values of difference between experimental curve and fitted curve for various polynomial orders at each inflation pressure .....	27
Table 2 Polynomial coefficients of fitted curves for each inflation pressure .....	28
Table 3 The eigenfrequencies and damping factors for each identified mode .....	30
Table 4 Coefficients of Fitted Polynomial curve of order 4 .....	35
Table 5 Comparison of computational times for envelope models with increasing number of cams .....	41

## Introduction

After the COVID-19 Pandemic, the public opted for sustainable micro mobility solutions that would help them avoid crowded public transport and became a convenient solution for shorter commutes. E- scooters became immensely popular and are still favored post pandemic due to their convenience and widespread availability of shared e-scooter services such as Lime, Bird, Tier etc. This arrival of e-scooters into mainstream means of transport has led to an increase in research into it's dynamics and ride comfort.

E-scooters are more lightweight than their traditional counterparts and have smaller wheels. Most e-scooters in the market also do not feature a suspension system. Since the rider would be exposed to the vertical dynamics more significantly in this case, it is pertinent to conduct a study on an accurate tire model to predict ride comfort and safety.

This thesis is based mainly on two well established tire models, namely the MF SWIFT envelope and rigid ring models. The obstacle envelope model helps to predict the tyre's filtering effect of smaller obstacles and gives an effective road profile. The rigid ring model is used to capture the tyre's dynamic response. A numerical simulation of the combined models is conducted in matlab. The results of which are compared to real world data collected from sensors attached to a e-cooter tyres, riding on a known road profile.

In the next section a brief literature review is presented on the topics of tyre modelling techniques and their development over the years.

# 1. Literature Review

## 1.1 Enveloping models

Since the 1960s research has been conducted on the performance of pneumatic tyres undergoing excitation from irregularities in road surfaces. Short irregularities garner more attention, since in this case, tyre deformation comes into play[1]. Many models have been developed to date that describe this enveloping behaviour and can be found in literature. Several of these as overviewed by authors Captain et al[2],Badalamenti et al[3] and Zegelaar[4] are as shown in figure 1.1[1]

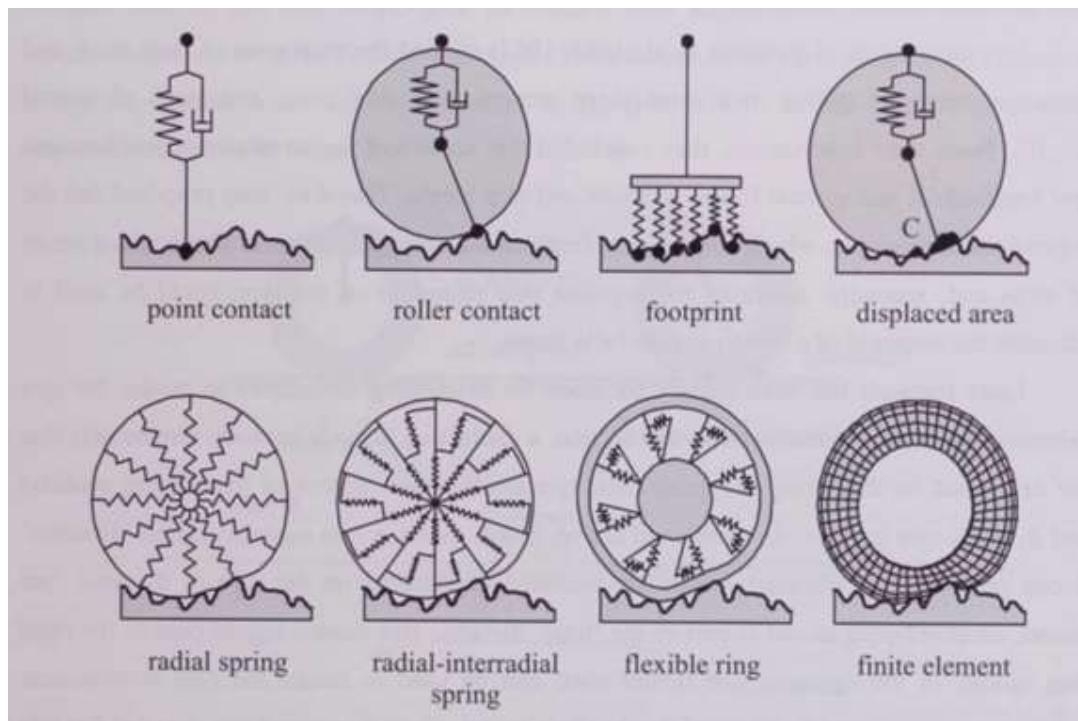


Figure 1.1 Several Envelope Models Found in Literature

The point contact model uses a spring damper system, and gives a good representation of forces developed when rolling over smooth surfaces, but fails on rough road surfaces. This is because it is incapable of accounting for the tyre's geometry and elasticity in its contact zone. This model is valid for road surfaces of wavelength much longer than the length of the contact patch[5].

The roller contact model too uses a spring-damper mechanism but also incorporates a rigid wheel. Therefore, the contact point is allowed to be not directly below the center. Although

it does filter out smaller bumps [3], the lack of accounting for tyre deformation leads to inaccurate modelling of the enveloping behaviour.

The radial spring model consists of springs in the radial direction, where forces are calculated at the wheel axle as a function of the spring deflection. The issue with this model was that since the springs' deflections were independent of one another, when the tyre was in a position where it was not completely supported by the ground or obstacle, the results were inaccurate. Consequently, the radial-interradial spring model was developed [3] where each radial spring was connected to its adjacent springs, by another spring. Badalamenti et al was able to show that this model could accurately describe aircraft tyre envelopment behaviour [3]. In the adaptive footprint model[2] the non-linear springs' deflection and the force due to constant inflation pressure acting over the adaptive footprint area give rise to the forces at the axle. This model can be considered a variant of the radial spring model [1].

The flexible ring models constitute of a flexible tyre tread and distributed sidewall stiffnesses. The tread band being allowed to bend means that the vertical stiffness at the center of the contact patch is lower than that at the edges. Therefore, these models can also show the typical dip in vertical force when rolling over obstacles. These models are, however, almost never used to investigate the quasi-static enveloping behaviour of tyres[1].

Footprint models use linear distributed stiffnesses and/or damping in the contact surface. Since tyre geometry in the zone of potential contact is not involved in this model, it is not very accurate. Displaced area models calculate the force as a function of the area of the unloaded tyre that intersects with the uneven road. This force acts along the centroid of the total displaced area and the wheel centre. Both types of models are better than the point contact model but show inaccuracies for roads with short and sharp obstacles.

### 1.1.1 The Development of Empirical Envelope Models

Key observations that led the development of empirical models was made by Bandel et al [6] who discovered that the vertical and longitudinal forces of a tyre rolling quasi statically over an obstacle could be described as the convolution of two identical basic functions, these basic functions were proven to be independent of the tyre inflation pressure or vertical load. Meanwhile obstacle height and length were shown to have an influence on them. Zegelaar[4] built upon this model and used quarter sine wave and half sine waves as basic functions for cleat and step obstacles respectively. Additionally, Zegelaar introduced the concept of the two-point follower moving over an elementary basic function, which would be an alternative to the convolution of the two basic functions, for a step obstacle. Schmeitz et al[7], [8] developed basic curves for some arbitrarily shaped obstacles and made some rules to get the basic profile for an arbitrary obstacle by summing elementary basic curves.

### 1.1.2 The Two Point Follower Model

Consider that the tyre rolls quasi statically over a step obstacle of height  $h_{step}$ , the tyre centre's vertical displacement is denoted by  $w$  and is the effective height. This can be obtained by the summation of two identical basic functions of length  $l_b$  that are at a distance of  $l_s$  and height  $(h_{step}) / 2$ .

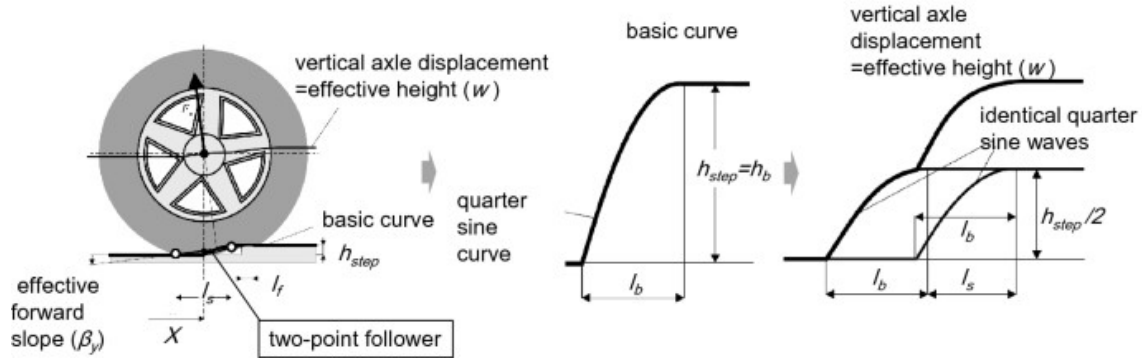


Figure 1.2. Representation of basic function and two-point follower models

According to the two point follower method introduced by Zegelaar [4], when the two points of the follower move along a single basic curve of height  $h_{step}$ , the midpoint of the line of length  $l_s$  connecting them describes the path of the effective height of the road. Apart from the parameters defining the basic curve, i.e.  $l_s$  and  $l_b$ , an additional parameter  $l_f$  determines the offset of the basic curve from the beginning of the step obstacle. The step responses from experimentation were fitted with two point follower method to determine the three parameters. Simultaneously these parameters were calculated for the case of a rigid unloaded wheel traversing the same obstacle.

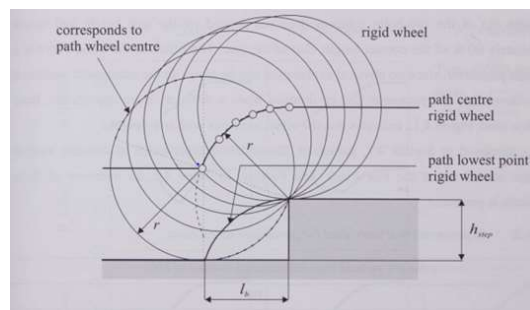


Figure 1.2. The rigid wheel response to a step obstacle

This led to the conclusion that the length of the basic curve  $l_b$  was almost independent of vertical load and corresponded well to that of the rigid wheel.

$$l_b = \sqrt{r^2 - (r - h_{step})^2} \quad (1)$$

It was also found that  $l_f$  the offset was dependent on the vertical load and that  $l_s$  didn't depend on step height and was about 80% of the tyre contact length.

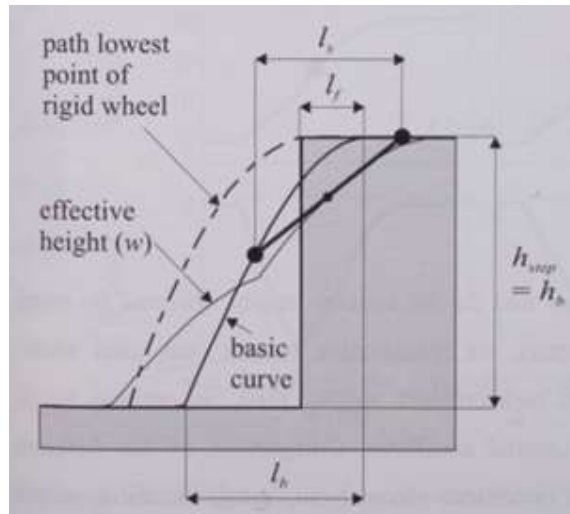


Figure 1.3 Comparison of Rigid Wheel and Quarter sine Basic Curves

Some rules developed to sum elementary basic curves to get the basic curve for an arbitrary obstacle, proved to be too difficult to execute for arbitrarily shaped road profiles. The use of the quarter sine basic curve and the offset  $l_f$  also led to complications.

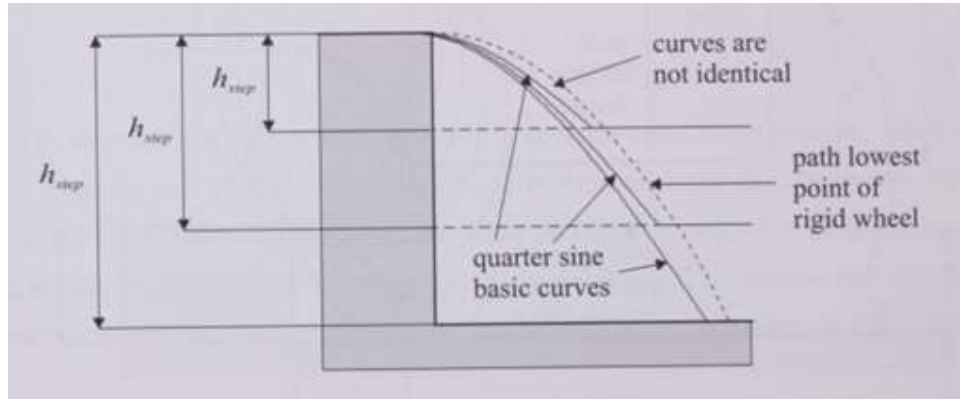


Figure 1.4 Quarter sine basic curves for three different step heights

Considering three different step heights, simulating the rolling of the tyre over this step obstacle, it stands to reason that since the tyre is unaware of the depth of the obstacle before it hits the ground, that all the basic curves should be the same. But as seen in the figure, this is not the case and it is caused by the offset which is dependent on step height and because the shape of basic curve used being the quarter sine curve. Therefore, use of the quarter sine wave is not ideal. Another basic curve that has no offset and follows the same path for different step heights as the rigid wheel does is required. This led to the development of the Tandem Elliptical Cam model.

### 1.1.3 Tandem Elliptical Cam Model

The new basic curve is developed using an elliptical cam. The lowest point of the ellipse is taken to generate the basic curve as it goes over a step obstacle. Since the elliptical basic curve needs to start at the same longitudinal position as the quarter sine model, it needs to have a shorter length than the length of rigid wheel response and hence have the shape of a standing egg[1].

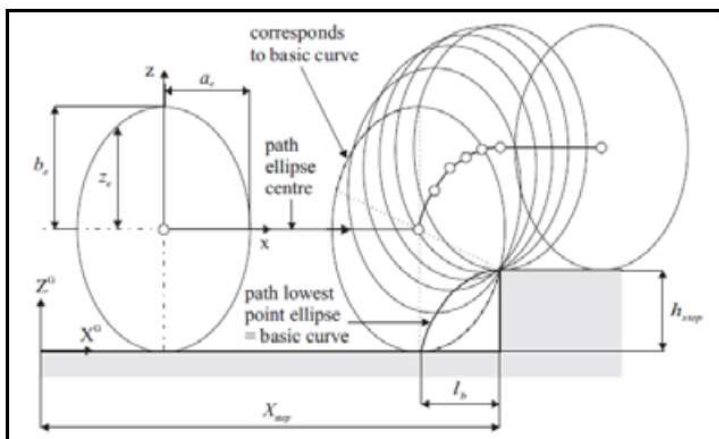


Figure 1.5 Basic Curve generated by elliptical cam

The shape of the elliptical cam is defined by parameters  $a_e, b_e$  and  $c_e$ . If  $x$  and  $z$  denote local coordinates, the ellipse equation is as follows

$$\left(\frac{x}{a_e}\right)^{c_e} + \left(\frac{z}{b_e}\right)^{c_e} = 1 \quad (2)$$

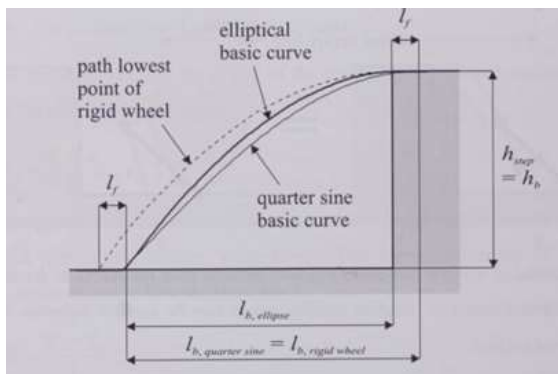


Figure 1.6 Comparison of elliptical and quarter sine basic curve

The elliptical basic curve follows the same curve regardless of the step height since the basic curve corresponds to the upper left part of the elliptical cam. Another point to notice is that the distance between the path of lowest point of rigid wheel and that of elliptical basic curve increases with step height, hence the offset of the Zegelaar model is accounted for.

The two-point follower can be used on this basic curve or for convenience it can be considered that two cams in tandem are moving along the actual road. These elliptical cams will be at a horizontal distance of  $l_s$  from the two point follower model. This model will be explained in detail in the second chapter.

## 1.2 Dynamic Tyre Model

The dynamic tyre model describes tyre behaviour such as displacement, velocity and acceleration considering the stiffness, damping and inertial properties of the tyre. Considering the various dynamic tyre models in literature, that accurately predict forces transmitted between tyre and wheel spindle, and have a reasonably low computational effort can be classified into four main categories[1]

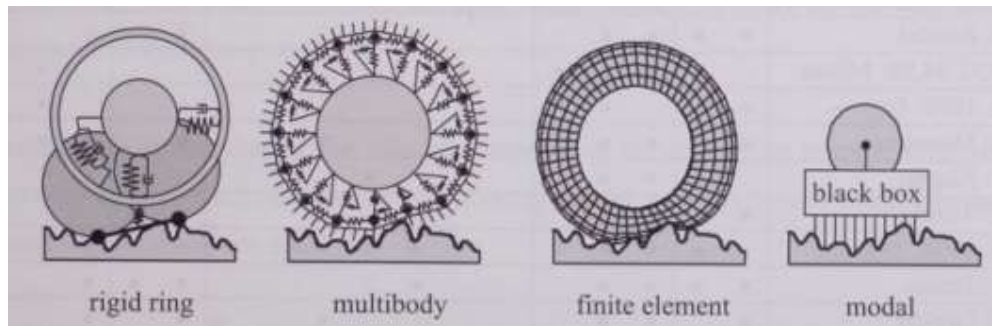


Figure 1.7. Different categories of Dynamic Tyre Models

### 1.2.1 Multibody Models

The first 3-dimensional version of the multibody tyre model was published by Eichler[9].

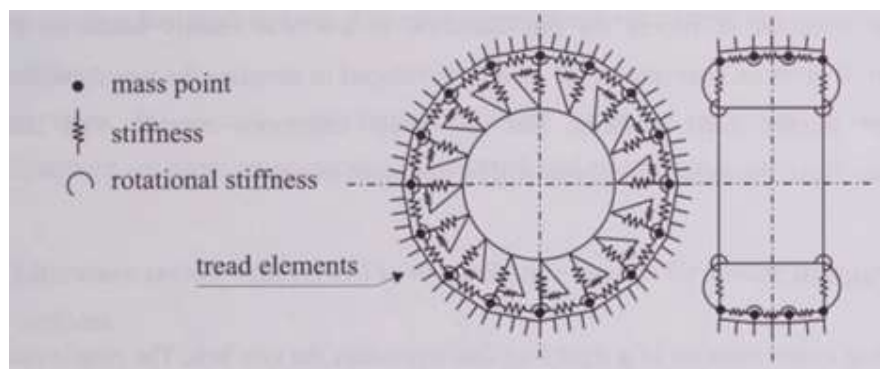


Figure 1.8. Three-dimensional Multibody Tyre Model

This model discretizes the tyre belt into a group of mass points that are interconnected by rotational and tension springs, which describe tyre belt elasticity. The sidewall mass is neglected and instead it connects the mass points of the belt to the rim of the tyre with dampers and radial and tangential springs. The tyre tread is modelled as a field of elastically deformable tread/brush elements. In the lateral direction the belt is discretized as a group of elastic rings involving mass points connected to each other via tension and rotational springs. The resistance of the belt to transverse displacements with respect to the rim and sidewall stiffness are described by rotational springs. Although commercial versions of this model are available, this model is not in popular use[1].

### 1.2.2 Finite Element Models

Finite element models are a very good to study the dynamic behaviour of tyres because they consider the materials and construction of the tyre, and can describe their influence on the behaviour of the tyre. Most publications [10], [11], [12] validate this model with experimental results of spindle forces when rolling over a cleat but the results are not much better with regard to the other categories of dynamic models[1]. Considering the high computational effort the FEM models demand, especially when long tracks of road are investigated, it is not worth choosing this model over others.

### 1.2.3 Modal Models

A modal model works like a 'black box'[1]. In this model, through modal dynamics of a tyre there is a coupling between contact patch input and spindle motion. Modal dynamics can be derived from either a finite element model of the tyre[13] or empirically from tests[6]. When this model uses modal dynamics obtained from finite element model, it cannot comprehend highly non-linear behaviour, like fractional loss of contact with the ground. Because of this it is more suitable to be used for roads of small unevenness like changes in texture, rather than bigger obstacles. Another disadvantage is that these models also do not involve a slip model so they can't be used for ride and handling simulations. But an advantage is they can be used for frequency of 250 Hz or more[13]. Hence modal models are more suitable for noise and vibration studies instead of ride and durability analysis[1].

#### 1.2.4 Rigid Ring Model

For a frequency range of 60-100 Hz , the deformations of the tyre belt can be neglected [1], [4], [14], therefore it can be considered as a rigid body. The rigid ring model represents the motions of the tyre where the belt remains circular, and flexible belt modes are neglected. The rigid ring is elastically suspended from the rim via spring-damper elements for all 6 degrees of freedom. This represents the sidewalls with pressurized air. In addition, there are residual stiffness elements between the contact model and the ring to obtain the correct total quasi static tyre stiffness. To describe the contact of the tyre with the road, a slip model and envelope model that gives effective road surface are required. In literature many different envelope models have been used in conjunction with the rigid ring model, but in this thesis the tandem model with elliptical cams will be used. Rigid ring model will be explained in detail in chapter 2.

## 2. MF Swift Model

The MF Swift model is comprised of four important elements [15]

- Magic Formula

The Magic formula developed by Dr. Hans B. Pacejka is an empirical model used to calculate the non-linear tyre forces and moments that occur in the tyre contact patch for different conditions of tyre loading and orientation.

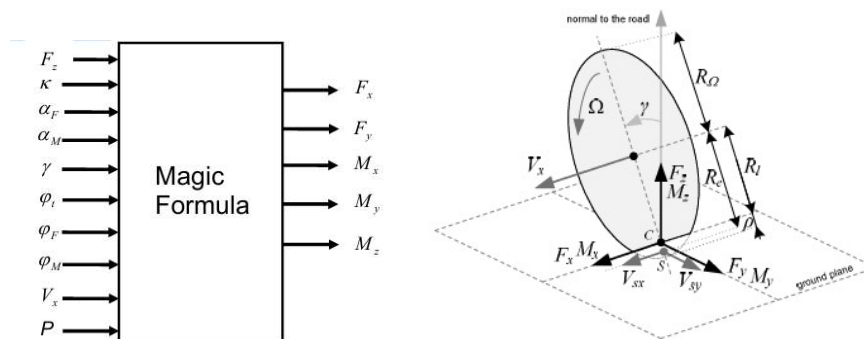


Figure 2. 1 Magic Formula inputs and outputs

- Contact Patch Slip Model

This model implements the transient behaviour of the tyre that depends on load and slip. The forces generated by the magic formula are applied to contact patch mass. This is then transferred to the wheel axle via a system of springs, dampers and the belt mass.

- Rigid Ring

Flexible modes of the belt are neglected and the belt mass is considered rigid and suspended elastically to the tyre rim. Additional stiffnesses are considered between the ring and contact to account for total quasi static stiffness.

- Obstacle Enveloping Model

The rigid ring model poses an important restriction that contact with the road surface should be at a single point. At this point magic formula is used to generate and apply the forces and moments. To accommodate this restriction, the concept of effective road surface is introduced to the model. It is assumed that the quasi static reaction of the tyre to a single point contact of the effective road is equivalent to the quasi static response of the real tyre on the real road surface. It is

also assumed that the local dynamic effects of the contact area can be neglected and that the tyre contact zone deforms dynamically the same way as it does quasi statically.[16]

## 2.1 Tandem Elliptical Cam Model

The tandem elliptical cam model comprises of two identical elliptical cams interconnected by a rod of horizontal length  $l_s$ . They are only allowed vertical motion as they move over the road surface.

The

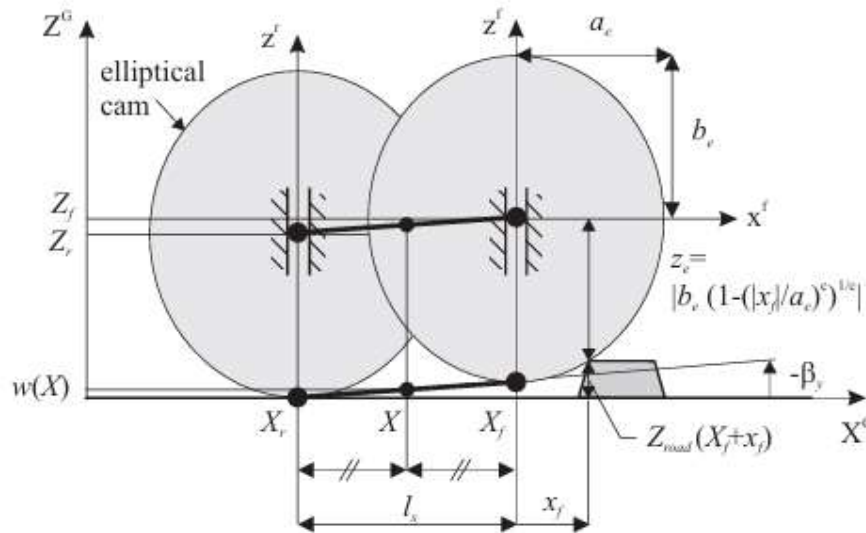


Figure 2. 2 Representation of Elliptical Cam Model generating effective road surface

midpoint of the rod connecting the bottom most points of the cams give the coordinates of the effective road surface.

The equation of the ellipse can be denoted by

$$\left(\frac{x}{a_e}\right)^{c_e} + \left(\frac{y}{b_e}\right)^{c_e} = 1 \quad (3)$$

Where  $x$  and  $y$  are local coordinates and  $a_e$ ,  $b_e$  and  $c_e$  are the shape parameters respectively.  $a_e$  and  $b_e$  are calculated as a function of the unloaded radius  $R_0$ , using some dimensionless

parameters that are obtained using extensive tyre testing and curve fitting [14], [17].  $c_e$  is also calculated using the same methodology[1]

$$a_e = l_e \cdot R_0 \quad (4)$$

$$b_e = h_e \cdot R_0 \quad (5)$$

$$l_s = 2 \cdot p_{ls} \cdot a \quad (6)$$

$z_e$  denotes the local z coordinate of the ellipse and is derived from the ellipse equation

$$z_e = \left| b_e \left( 1 - \left( \frac{|x|}{a_e} \right)^{c_e} \right)^{\frac{1}{c_e}} \right| \quad (7)$$

To get the height of the ellipses as they traverse the ground, consider the largest vertical overlap between the ellipse and the road profile, if one considers the ellipse to move at the ground level. The ellipse will just touch the road at this point. In matlab, the height of the points of lower half of the ellipse can be checked with the road height. Increased discretization of the points give better results. From this we can describe the global height of the ellipse as follows

$$Z = \max \left( z_r(X + x_f) + z_e(x_f) \right) \quad (8)$$

Where  $X$  denotes ellipse global x coordinate and  $x_f$  denotes local x coordinate of each point on the lower ellipse half that is checked, with respect to ellipse center. If  $Z_f$  denotes the vertical coordinate of front ellipse center and  $Z_r$  denotes corresponding rear ellipse center, the height of the midpoint of the rod connecting their bottom most point  $w$  is given by

$$w = \left( \frac{Z_r + Z_f}{2} \right) - b_e \quad (9)$$

In the 3d version of the tandem elliptical cam model, the cams can be visualized as populating the boundary of the contact patch. Cams can be arranged parallelly to the original model in the axial direction, in multiple evenly spaced tracks till it reaches the end of the contact patch on the other side. The number of cams in the longitudinal direction may

be increased for the two side edges of the contact patch as well. This would increase accuracy at short wave length obstacles[15]

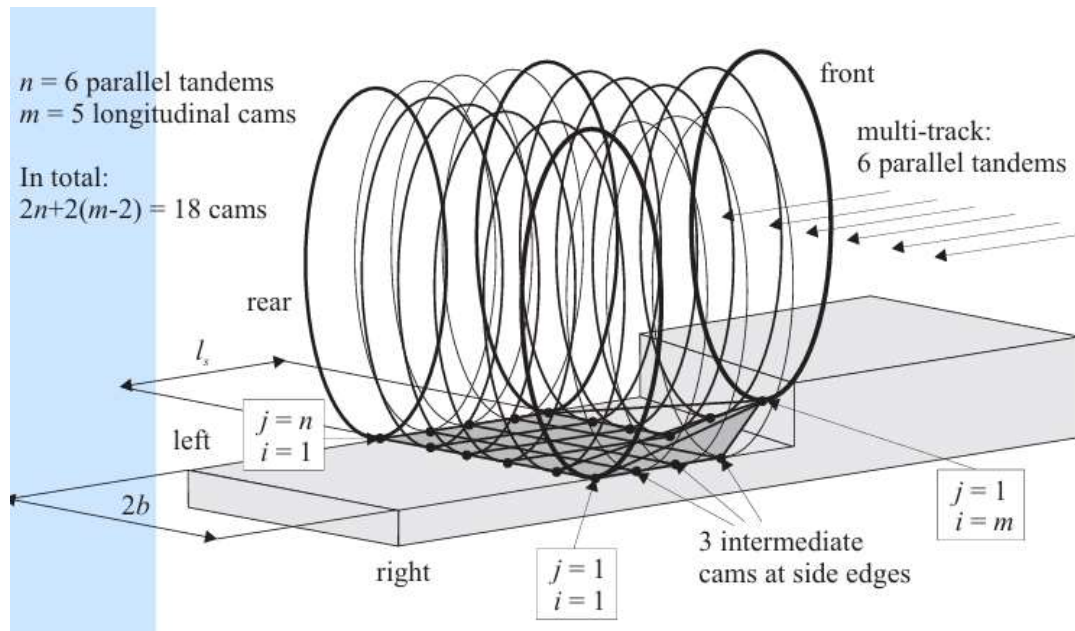


Figure 2. 3 Diagram of 3-dimensional tandem elliptical cam model depicting cam arrangement

The modified height is calculated by subtracting the ellipse height from the mean height of all the cams. Since this thesis is limited to the vertical analysis of the tyre, the 2D version with only the longitudinal cams may be considered.

## 2.1.1 Cam Properties Evaluation

An alternative method of describing parameters ellipse length  $a_e$  and tandem base length  $l_s$  is found in literature[18] , where they are a function of the contact length.

$$a_e = R_0 - \xi \cdot a \quad (10)$$

$$l_s = 2a\xi \quad (11)$$

Here  $\xi$  represents the footprint fraction and  $R_0$  is the unloaded tyre radius. So it follows from (10) and (11) that the centers of the elliptical cams and the center of the tyre align on the diameter of the circle. We also know that the cams are along the edge of the contact footprint.

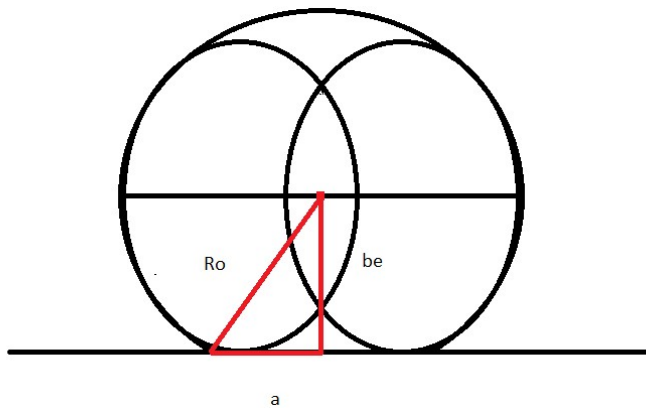


Figure 2. 4 Diagram of Tandem Model with loaded tyre indicating relation of paramters  $R_0$ ,  $a$  and  $b_e$

From this relation, one can obtain  $b_e$

$$b_e = \sqrt{R_0^2 - a^2} \quad (12)$$

Experiment results [1] show that the shape of elliptical cams of the tandem model show a good correspondence to the outside contour of the loaded tyre , in the zone where possible contact with obstacles takes place.

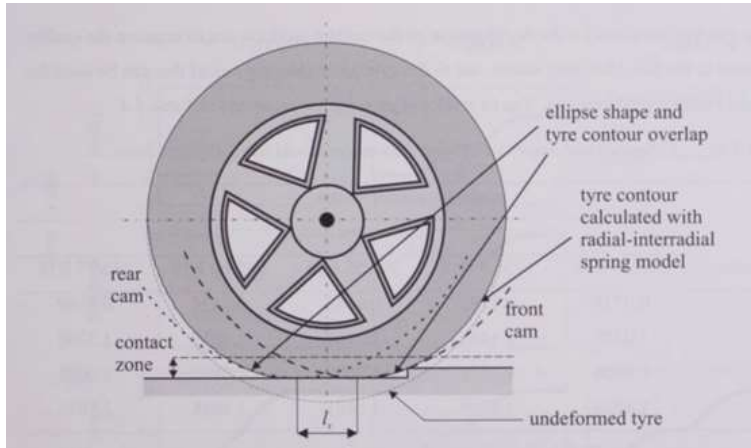


Figure 2. 5 Comparison of outside contour of loaded tyre and Tandem model ellipse shape in zone of possible contact

To summarize, one could obtain the value of  $b_e$  given the values of unloaded radius and footprint length and utilizing the shape correspondence, the values of  $c_e$  and  $a_e$  can also be found by running an optimization code in Matlab. An example is shown below for random values of  $R_0$  and  $a$

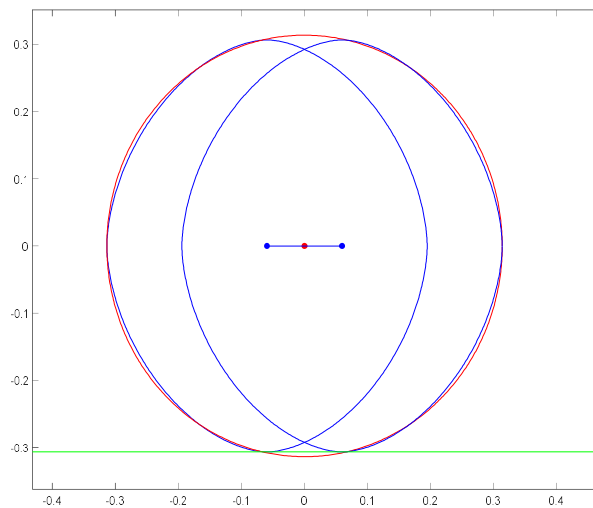


Figure 2. 6 Result of the matlab code to fit the elliptical cam shape to tyre outside contour for a given unloaded tyre radius and footprint length

The program was designed to accept values for  $R_0$  and  $a$ , and to calculate  $a_e$ ,  $b_e$  and  $c_e$  to maximize shape correspondence in the zone of possible contact.

## 2.2 Rigid Ring Model

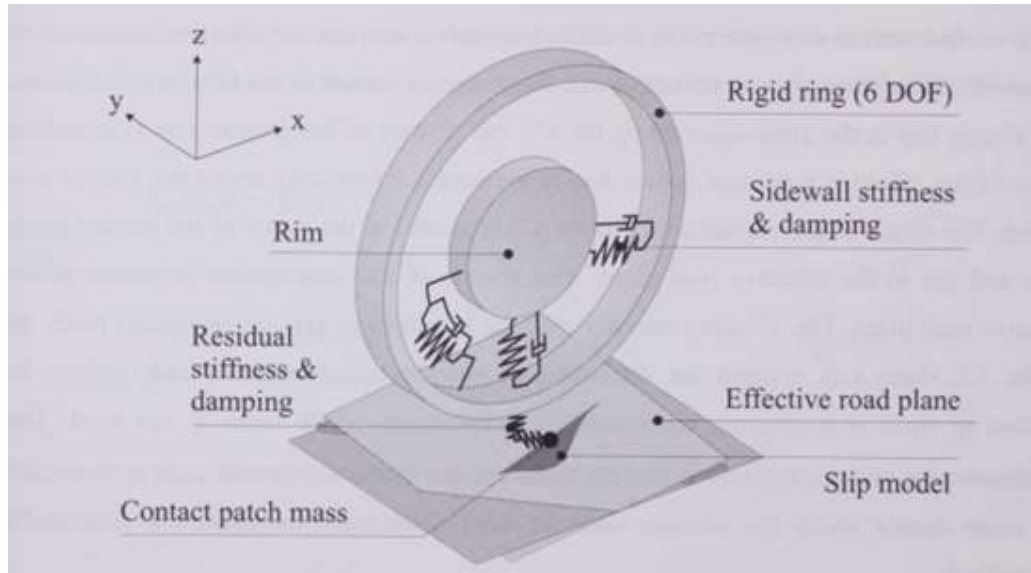


Figure 2. 7 The rigid ring model featuring the rigid ring, flexible sidewalls, the contact model which includes a small contact mass, slip model and residual stiffness and damping elements

For the investigation of vertical dynamics, a simplified model may be used to describe the tyre[15]

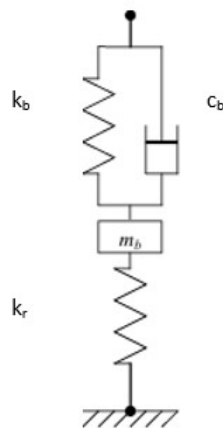


Figure 2. 8 Simplified system to describe tyre vertical dynamics

Here  $k_b$  and  $c_b$  represent belt stiffness and damping properties respectively. Modal analysis is conducted on the tyre to find its longitudinal frequency from which these values can be derived.  $K_r$  represents the residual stiffness between the road and the tyre so that overall quasi static stiffness is maintained.  $m_b$  is the tyre belt's mass. If  $f_{long}$  denotes the tyre longitudinal frequency and  $\zeta_{long}$  the corresponding damping factor, the following equations describe  $k_b$  and  $c_b$

$$k_b = 4\pi^2 m_b f_{long}^2 \quad (13)$$

$$c_b = 4\zeta_{long} \pi f_{long} m_b \quad (14)$$

In this thesis, the experimental results have been derived from a human riding an e-scooter on a known road profile, with sensors attached to the scooter to read the data. Hence the model is modified to add the human as the 3<sup>rd</sup> degree of freedom.

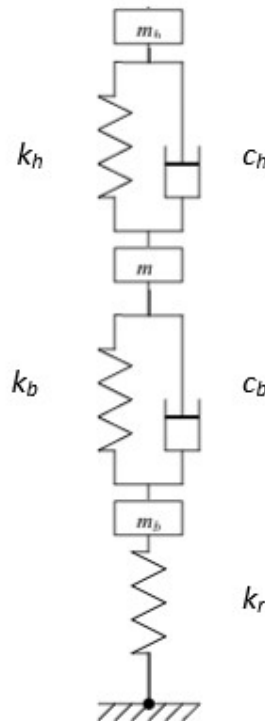


Figure 2. 9 Three degree of freedom tyre vertical dynamics model

$m$  denotes the mass of the e-scooter apart from that of the belt.  $m_h$  is the mass of the human rider and  $c_h$  and  $k_h$  denote the corresponding damping and stiffness values.

The equations of motion for the three dof model are as follows, where  $z$ ,  $z_b$  and  $z_h$  are the vertical displacements of the tyre rim, belt, and human respectively

$$m_h \ddot{z}_h + c_h (\dot{z}_h - \dot{z}) + k_h (z_h - z) + m_h g = 0 \quad (15)$$

$$m \ddot{z} + c_b (\dot{z} - \dot{z}_b) + k_b (z - z_b) + c_h (\dot{z} - \dot{z}_h) + k_h (z - z_h) + m g = 0 \quad (16)$$

$$m_b \ddot{z}_b + c_b (\dot{z}_b - \dot{z}) + k_b (z_b - z) + k_r (z_b - z_r) + m_b g = 0 \quad (17)$$

The basic idea of the combined envelope and rigid ring model is that the envelope model provides the effective road height to the rigid ring model, which in turn calculates the road reaction force which in turn provides the contact patch dimensions which decide the cam properties for the envelope model. This forms a cycle of constant feedback which is represented in the diagram below

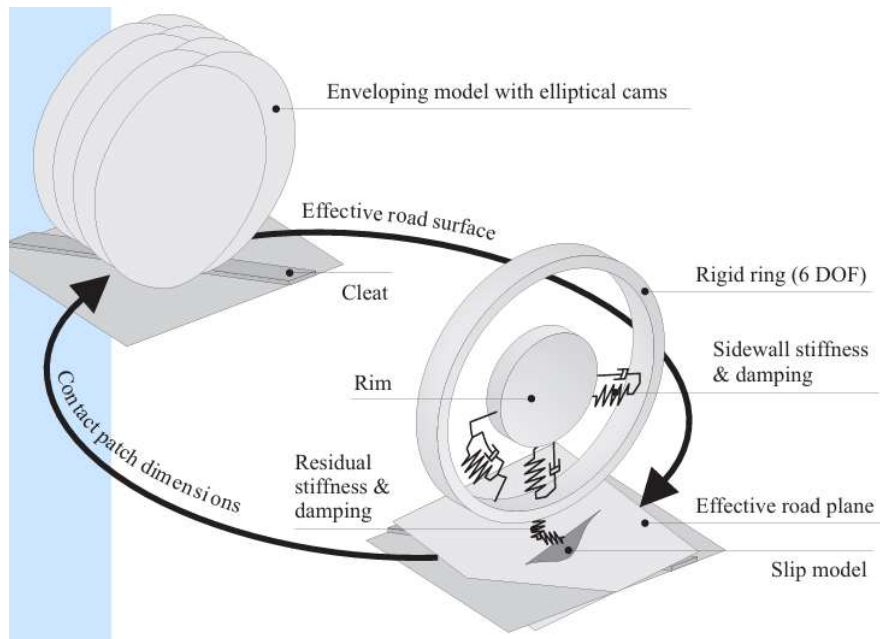


Figure 2. 10 Feedback cycle between enveloping model and rigid ring model that forms the basis for evaluating the vertical dynamics of the tyre

### 3. Experiments

The model requires several experimentally derived parameters, namely the belt and residual stiffnesses and the belt damping. It also requires data of contact patch dimensions corresponding to applied force. To this end several experiments were conducted and the data recorded for use.

#### 3.1 Radial Stiffness Test

The experiment is conducted on the tyre of a Xiaomi Pro II electric scooter tyre, to evaluate its radial stiffness. It is fixed onto a rig that keeps it in place and prevents rotation about its own axis. It is then attached onto an MTS machine, above which is a load cell connected to an adaptor that moves in the vertical direction, controlled by the machine. The exerted load, and displacement of the crossbar are recorded by the system.



Figure 3. 1 Experimental setup of tyre on MTS machine for radial stiffness evaluation

The principle behind the test is that by plotting the load exerted as a function of the vertical tyre displacement, the derivative of the curve will give radial stiffness. Hence, we should be able to plot the total radial stiffness of the tyre with respect to the load exerted on it, or with respect to the total vertical displacement of the tyre.

$$k = \frac{dF_z}{dz} \quad (18)$$

The test is conducted for 5 different levels of inflation pressure, each pressure level tested thrice to check for repeatability. The load limit is set to 1000 N as the total weight of the e-scooter and human is less than 100kg, which would be distributed among the front and rear tyres. So, it's safe to assume that upper limit for the vertical load is limited to 1000 N.

The procedure of the test begins by adjusting the experimental setup so that the adaptor is centered with respect to the tyre. The nominal pressure of the tyre is found to be 3.5 bar, so 2 values of pressure above and below it will be tested along with the nominal pressure. An electric compressor is used to modify the tyre inflation pressure. The test is run to a limit of 1100 N so that experimental data at 1000 N is unaffected by irregularities. The test is run three times so they can be plotted together to check for repeatability, for each of the inflation pressures 2.5 bar, 3.0 bar, 3.5 bar, 4 bar and 4.5 bar.

### 3.1.1 Post Processing and Results

The raw experimental data is obtained in a .txt file and extracted to matlab, an example plot is given below

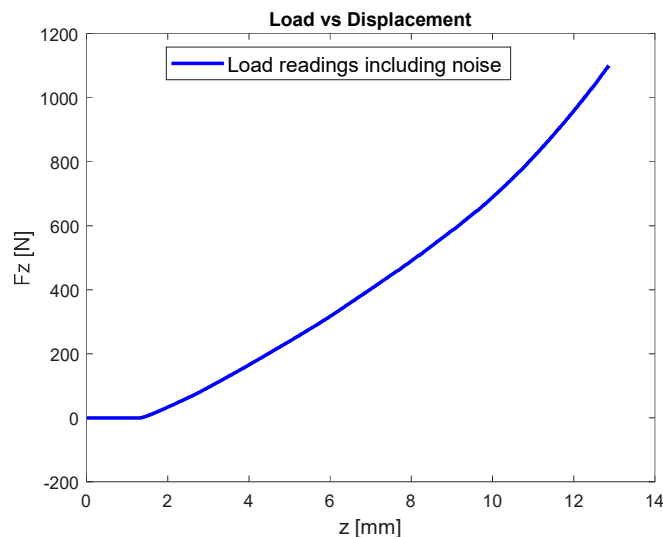


Figure 3. 2 Plot of Raw Experimental Results

The readings also include noise values and they need to be removed for accurate calculations. To obtain tyre displacement from the recorded values of crossbar displacement, the initial load value is taken to be the point at which load is just above the maximum load noise value recorded, the load reading at this point and the displacement corresponding to it are subtracted from the remaining load and displacement readings respectively, so the initial reading is 0 mm displacement at 0 N force. Also since the experiment is limited to an upper limit of load of 1000 N, values recorded above this limit are trimmed, resulting in a changed plot as follows

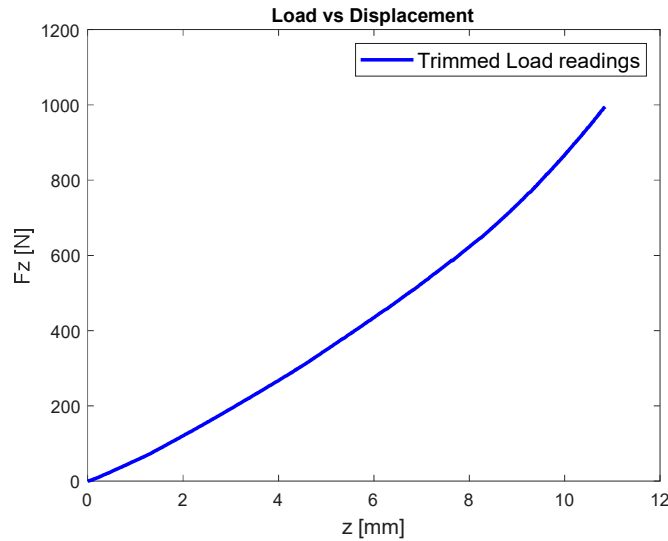


Figure 3.3 Plot of Experimental data after deleting noise values and setting upper limit

For each inflation pressure, three tests were conducted to check repeatability of the readings. They need to show a good agreement for the readings to be acceptable.

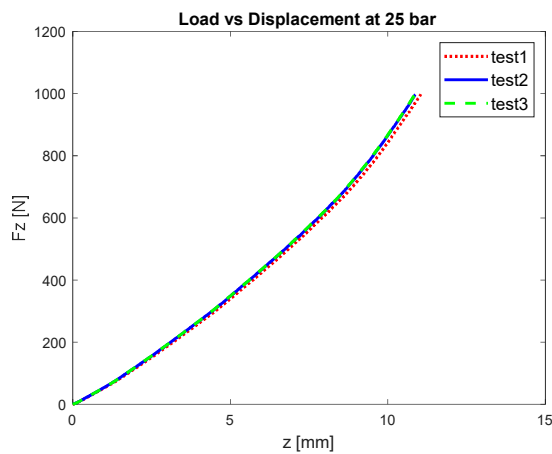


Figure 3.5 Plot of three separate test results for Load vs displacement at 25 bar inflation pressure

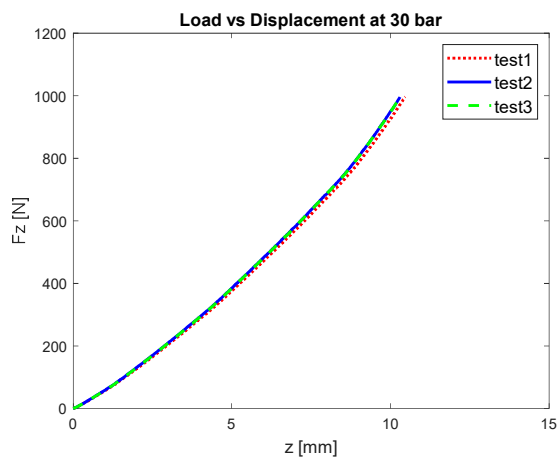


Figure 3.4 Comparison of experimental data with fitted curves of various polynomial orders at 30 bar inflation pressure

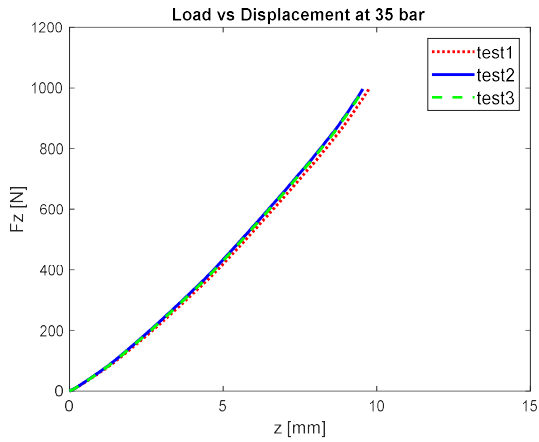


Figure 3. 6 Plot of three separate test results for Load vs displacement at 35 bar inflation pressure

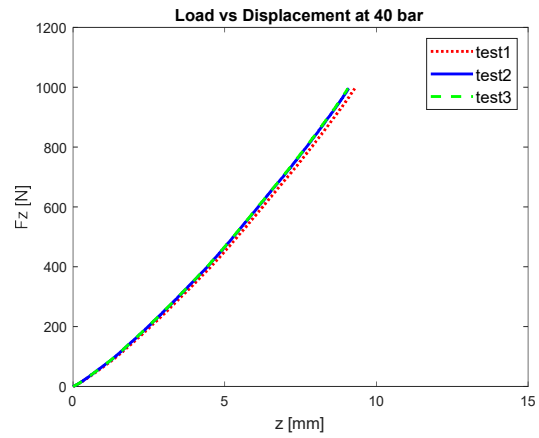


Figure 3. 8 Plot of three separate test results for Load vs displacement at 40 bar inflation pressure

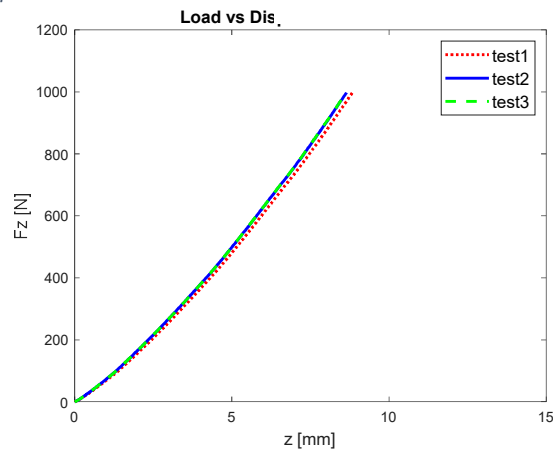


Figure 3. 7 Plot of three separate test results for Load vs displacement at 45 bar inflation pressure

Using polyfit in matlab, we can fit a polynomial to the curve of the experimental data. The following are couple of examples of the results when polyfit is attempted with different orders 'n', where the polyfit curve is of the form

$$p_1x^n + p_2x^{n-1} + p_3x^{n-2} + \dots \dots \dots p_n \quad (19)$$

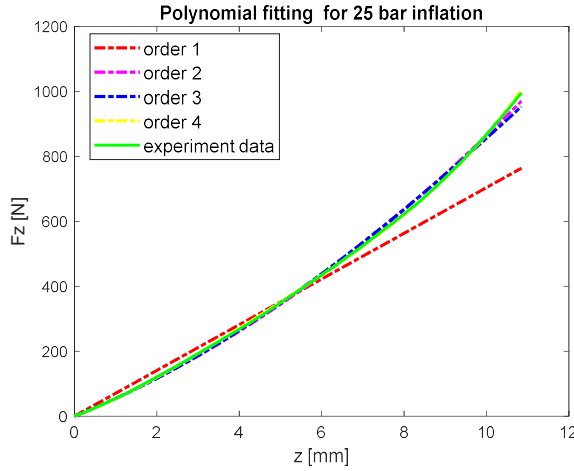


Figure 3. 10 Comparison of experimental data with fitted curves of various polynomial orders at 25 bar inflation pressure

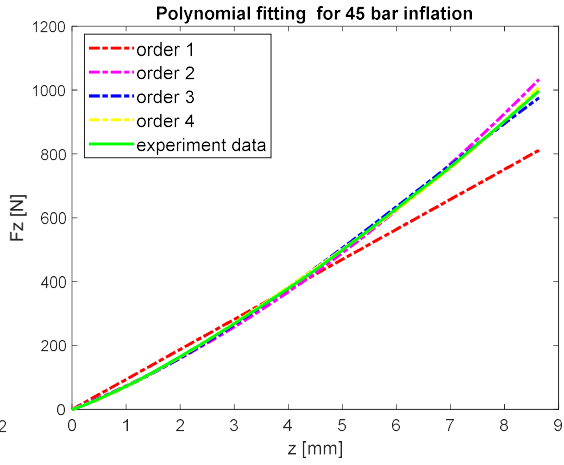


Figure 3. 9 Comparison of experimental data with fitted curves of various polynomial orders at 45 bar inflation pressure

In

all the cases, polynomial of order 2 matches the experimental data well enough without increasing the order too much . The RMS values of differences between the fitted curves and the experimental plots for each order of polynomial is as follows

Table 1 RMS values of difference between experimental curve and fitted curve for various polynomial orders at each inflation pressure

Inflation Pressure [bar]	order of polynomial			
	1	2	3	4
45	72.24	12	5.83	3.14
40	72.2	11.95	6.12	3.48
35	73.03	11	7.25	3.54
30	72.68	7.94	9.26	2.35
25	75.011	7.8624	10.44	2

Therefore, the force can be obtained as a function of vertical displacement as follows

$$F_z(x) = p_1 z^2 + p_2 z + p_3 \quad (20)$$

From which stiffness can be obtained as

$$k(x) = 2p_1 z + p_2 \quad (21)$$

The following table gives the values of the polynomial coefficients for each level of inflation pressure

Table 2 Polynomial coefficients of fitted curves for each inflation pressure

Inflation Pressure [bar]	p1	p2	p3
45	5.95	68.18	0
40	5.4	64.54	0
35	4.86	59.79	0
30	4.01	55.1	0
25	3.52	51.25	0

Now that total radial stiffness can be plotted with respect to displacement, the plot for the 5 different inflation pressures is as follows

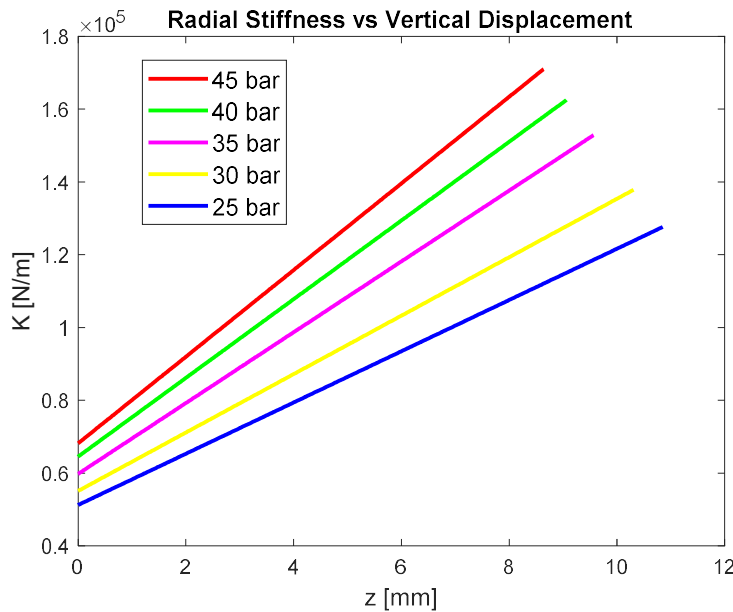


Figure 3. 11 Plot of Radial Stiffness as a function of vertical displacement for each inflation pressure

The total radial stiffness is a result of the belt stiffness and residual stiffness. In a quasi-static state, these springs are in series connection and the total stiffness can easily be calculated as

$$\frac{1}{k_{tot}} = \frac{1}{k_{belt}} + \frac{1}{k_{residual}} \quad (22)$$

Now that total radial stiffness is identified, the next step to experimentally determine the belt stiffness, which is a function of the tyre's eigenfrequency. To this end modal analysis is performed on the tyre, as explained in the next section.

### 3.2 Experimental Modal Analysis

The objective of conducting the experimental modal analysis is to evaluate the different tyre modes. The radial modal frequency and damping values are required to evaluate the belt stiffness and damping. This experiment is conducted using the Siemens Simcenter Test lab, (formerly LMS Test Lab) which reads and analyzes the tyre response to excitation and helps to extract the modes from this data.

The tyre of a Xiaomi Pro II electric scooter is marked around the tread, sidewalls, and rim at regular intervals to denote different nodes. An impact hammer is used to excite these nodes, the response is captured by accelerometers placed at the rim, tread, and sidewalls. The hammer and accelerometers are connected by wires to the SCADUS hardware. Small nuts are glued on at the nodes for hammering, this provides a better reading of the excitation.



*Figure 3. 12 Tyre setup for Experimental Modal Analysis*

The tyre setup is hung from a crane by the means of elastic rubber bands. Initial rounds of testing did not present favourable results and it was understood that the mass of the accelerometers was interfering with the result so setup was modified to include smaller and lesser number of accelerometers.

The test is conducted on an unloaded tyre in free-free conditions. Rigid ring modes identified are ignored since they only describe properties of the rubber band used to hang the tyre.

### 3.2.1 Post Processing and Results

The initial estimates of the modal frequencies are done using the peak picking method. The response of the tyre and input are used to create a Frequency Response Function. The peaks in this frequency domain plot may point to possible natural frequencies. Selecting a few possible options and a trial modal order, the stabilization diagram is employed.

Stabilization diagrams are used when the exact modal order is unknown. It features the modal frequencies calculated for each modal order on a plot where the x axis denotes frequency and y-axis, the number of modes. The order of modes chosen is typically high, to try and capture all relevant characteristics of the structure.

However, because of this overestimation of nodes, there may be several mathematical poles that are not physical, along with the physical poles. Physical poles tend to line up at nearly identical frequency along the number of nodes, but the mathematical poles are scattered around the frequency range. Hence, we can distinguish between them and can select likely modal frequencies. A typical stabilization diagram can be as follows

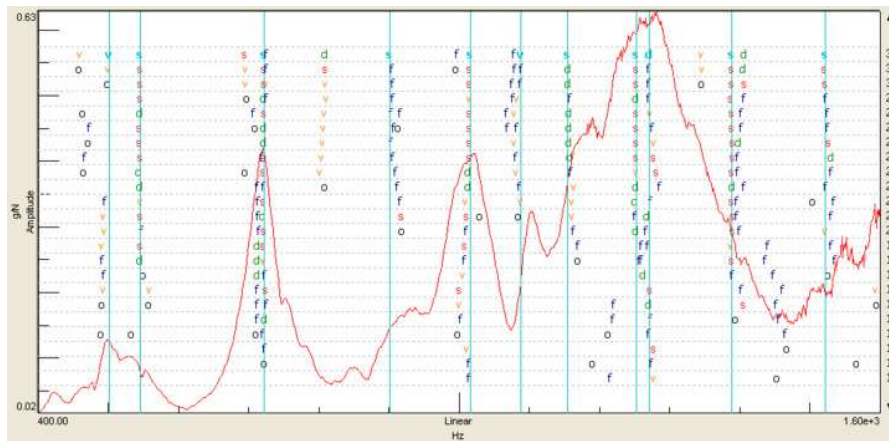


Figure 3. 13 Example of a stabilization diagram

Each of these possible modes can be animated to check for expected mode shapes. As a result 5 different modes where tyre tread is undeformed are identified. Their natural frequencies and damping coefficients are given in the following table.

Table 3 The eigenfrequencies and damping factors for each identified mode

Mode	Eigenfrequency [Hz]	Damping Factor
1	334.698	0.0727
2	508.5954	0.0741
3	524.011	0.0818
4	608.3501	0.0048
5	610.3688	0.0047

The modal data including eigenfrequencies, modal shape and damping factor, and data regarding the structure and nodes of the tyre are fed to 'Lupos', an FEM visualization tool developed by a team in Politecnico Di Torino lead by Prof. Elvio Bonisoli.

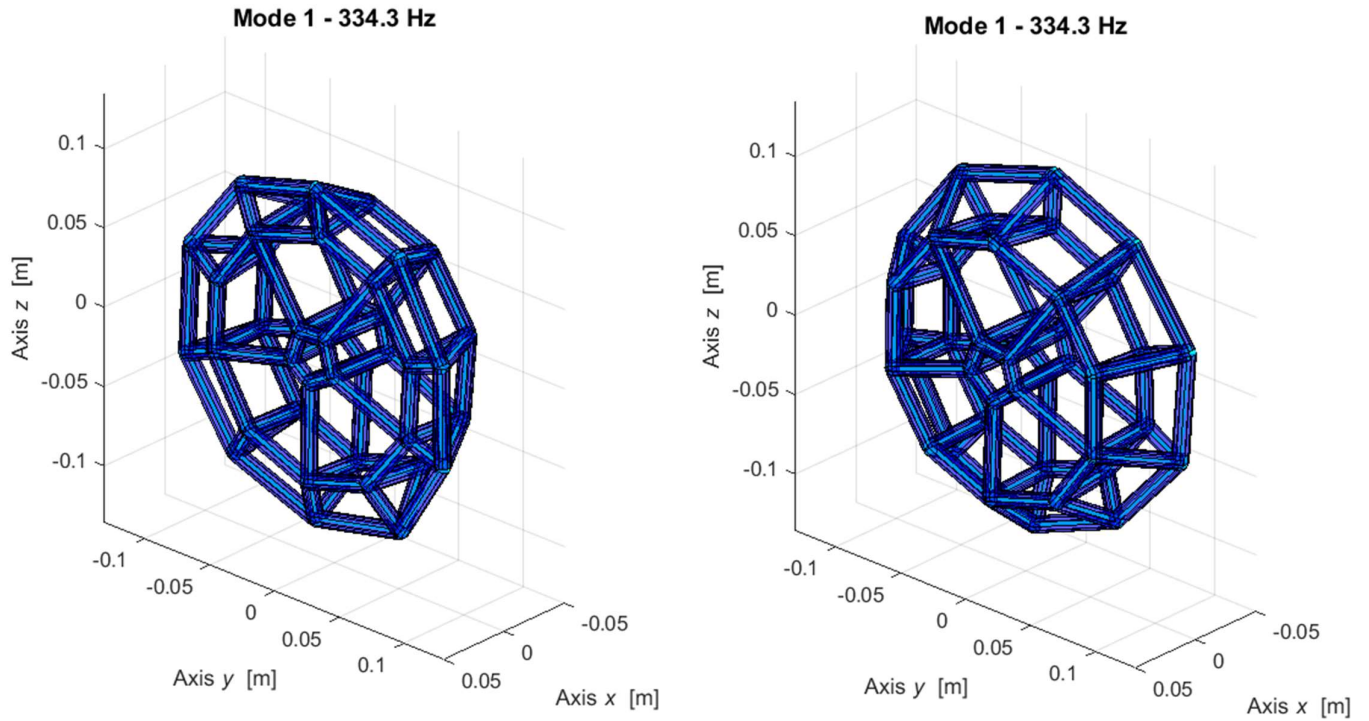


Figure 3. 15 First Modal Shape identified at 334.3 Hz

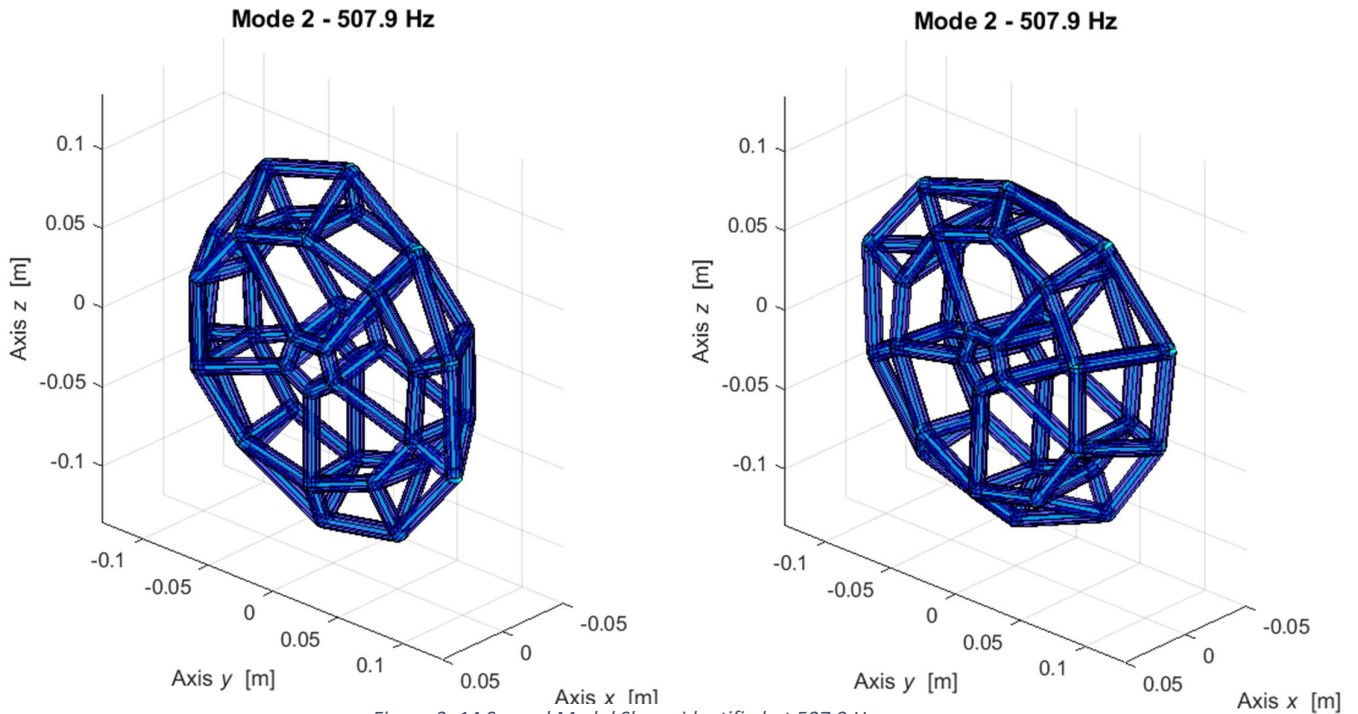


Figure 3. 14 Second Modal Shape identified at 507.9 Hz

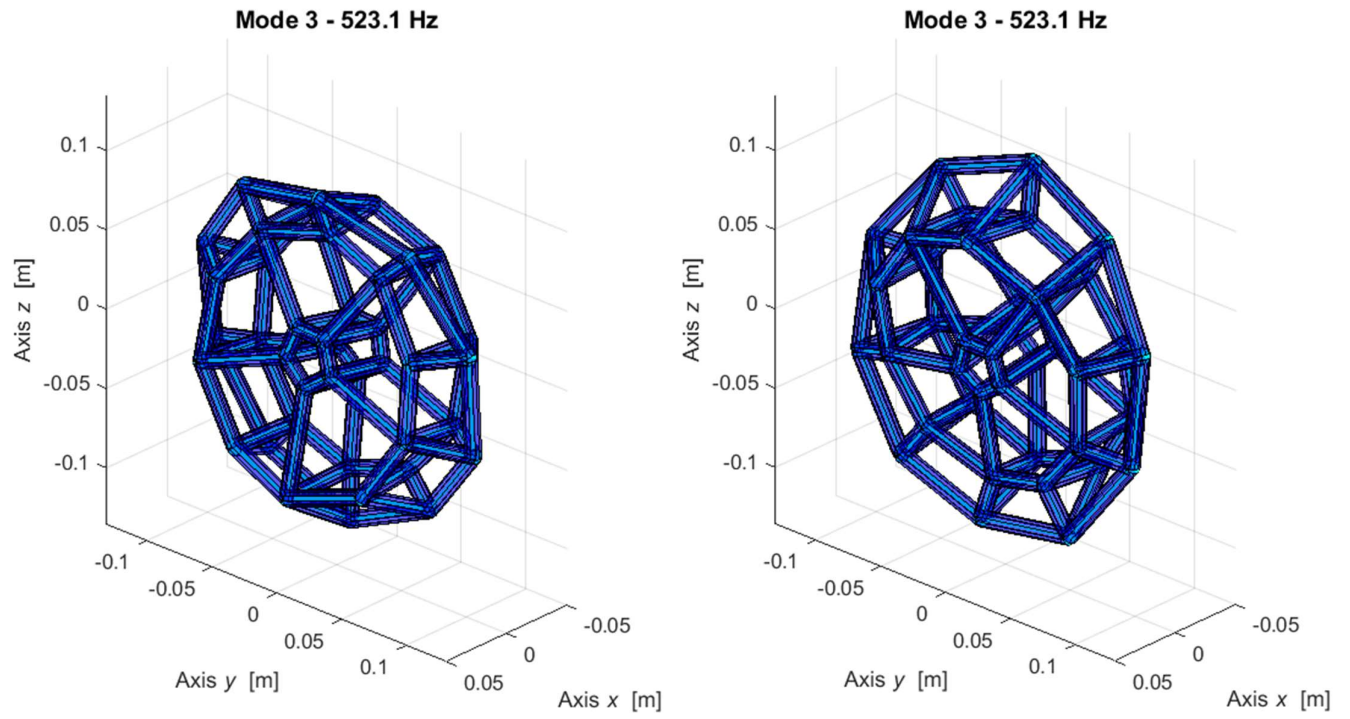


Figure 3. 16 Third Modal Shape Identified at 523.1 Hz

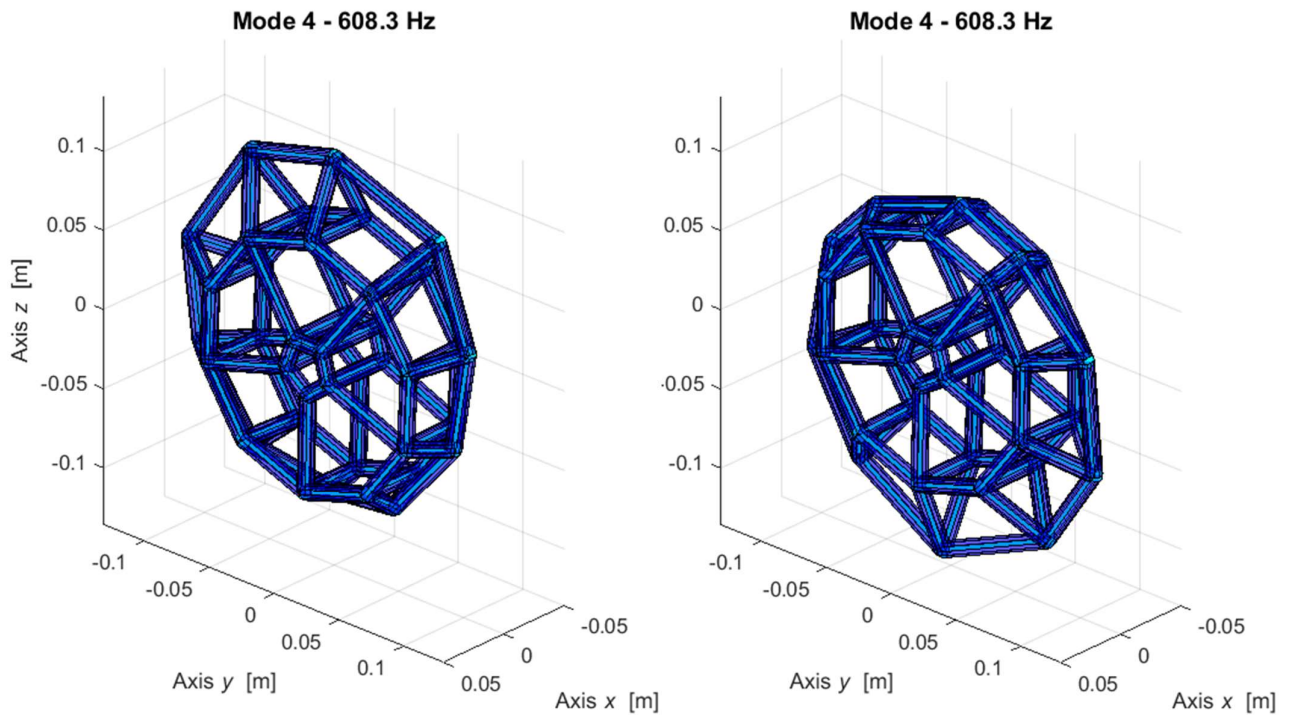


Figure 3. 17 Fourth Modal Shape identified at 608.3 Hz

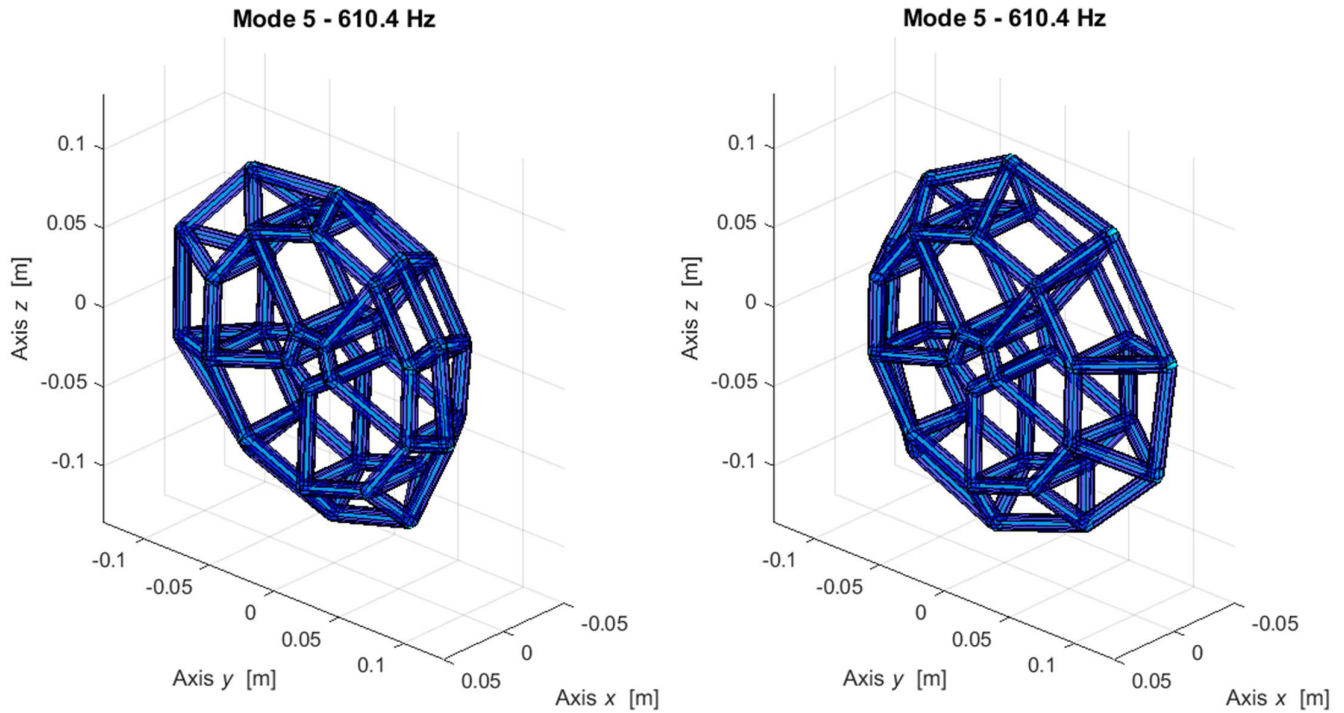


Figure 3. 18 Fifth Modal shape identified at 610.4 Hz

The fourth mode is identified as the radial mode. With the corresponding eigenfrequency and damping ratio, used in equations (13) and (14) the belt stiffness and damping can be calculated.

Now with both the belt stiffness and the total radial stiffness, using equation (22) the residual stiffness corresponding to the vertical displacement of the tyre may be obtained. Since  $k_b$  is much stiffer than  $k_r$  and contributes little to the overall tyre displacement, one may attribute the total vertical displacement to the residual stiffness and plot it so.

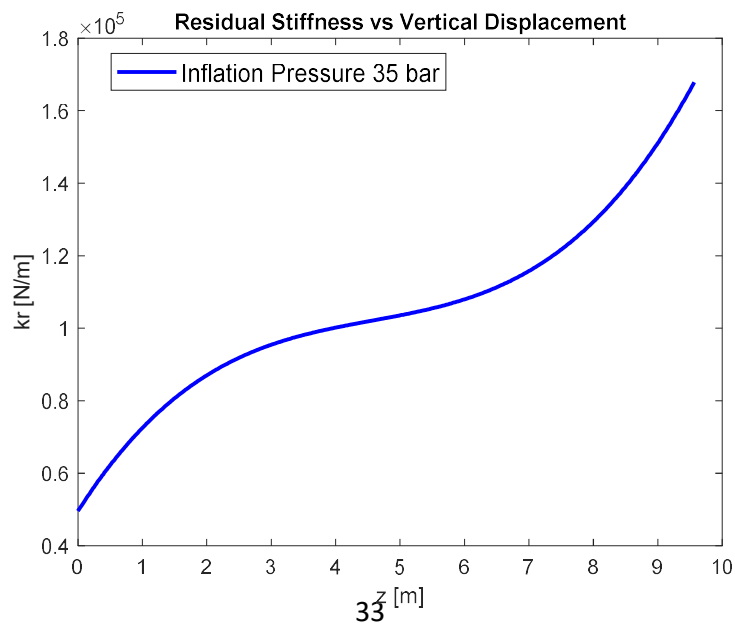


Figure 3. 19 Plot of Residual Stiffness as a function of total vertical displacement at 35 bar inflation pressure

### 3.3 Footprint Analysis

The contact patch dimensions are key to determine the properties of the elliptical cam used in the envelope model. The objective is to obtain the contact patch dimensions as a function of the applied vertical load. The experimental setup involves fixing the tyre onto the MTS machine which can apply the vertical force in increments.

Fujifilm prescale paper is pressure sensitive film coated paper that changes colour to red on the application of pressure. This paper can be placed on the horizontal surface where the tyre makes contact to capture the contact patch. Different types of the prescale paper are suited to different pressure ranges. In order to determine the possible pressure range, a rough sketch of the contact patch can be made by pencil on paper to calculate its nominal area and using the force range of the experiment, the pressure range is obtained.

A couple of examples of the experimental result obtained is as follows

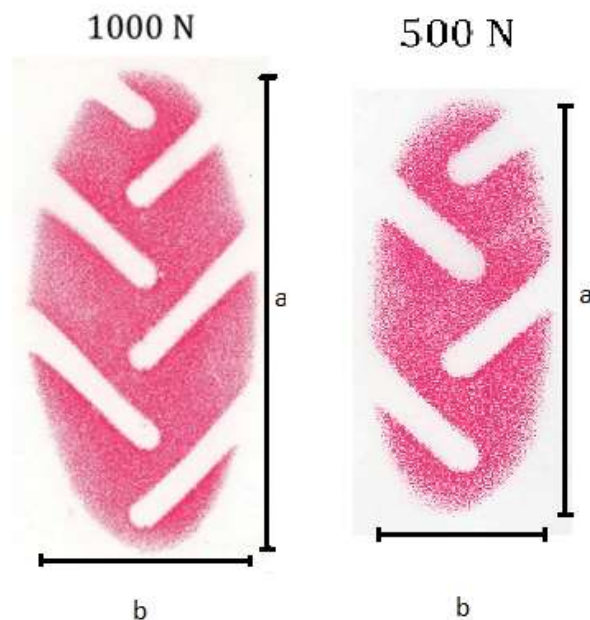


*Figure 3. 20 Footprint captured of 35 bar pressure tyre at Loads of 1000 N and 500 N on Fujifilm prescale*

The parameters  $a$  and  $b$  denote the contact patch length and width respectively. These values can be plotted for each increment in load as follows

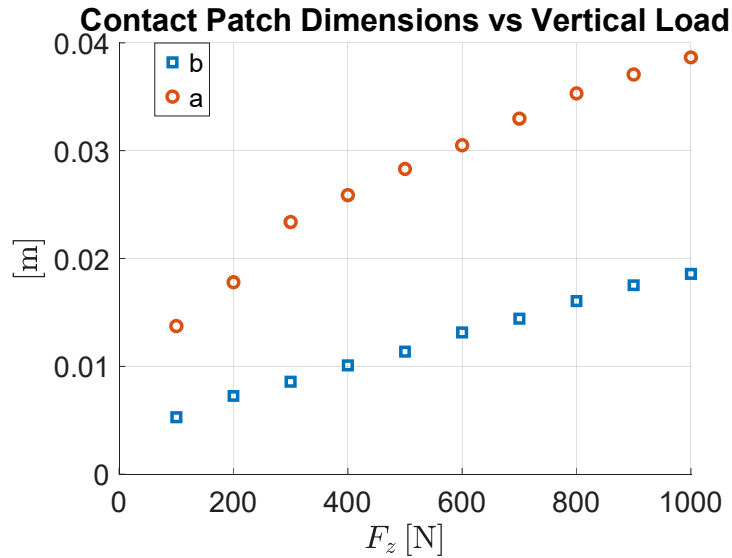


Figure 3. 21 Plot of Contact patch dimensions measured at each Vertical Load input

The scope of this thesis is limited to the vertical dynamics of the tyre, hence only the contact patch length is of importance. The experimental data can be best fitted with a polynomial curve of order 4, where the contact length is expressed as a function of vertical force as follows

$$a = p_1 F_z^4 + p_2 F_z^3 + p_3 F_z^2 + p_4 F_z + p_5 \quad (23)$$

Table 4 Coefficients of Fitted Polynomial curve of order 4

p1	p2	p3	p4	p5
-3.91E-14	1.08E-10	-1.17E-07	8.01E-05	0.006525

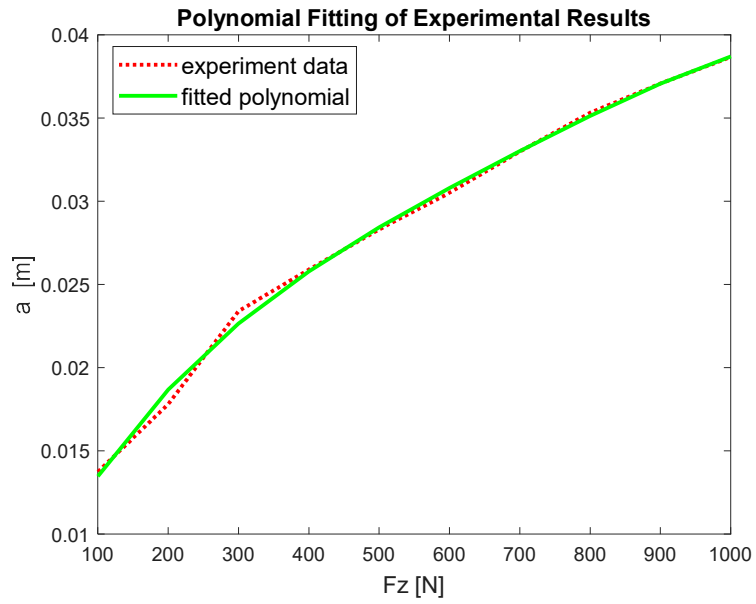


Figure 3. 22 Plot of experimental results and corresponding fitted polynomial curve of contact footprint length vs Vertical load

## 4. Modelling

### 4.1 Envelope Model Results

The Envelope model is developed to accept road coordinates to build the corresponding effective road profile. Since the no. of cams can be increased for better results, the model is adapted to do the same. The results for a few basic road profiles are evaluated for a 2 cam model

#### *Step obstacle*

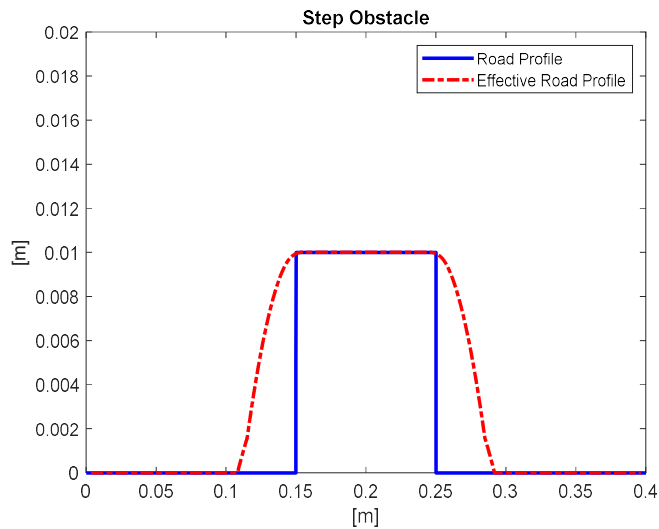


Figure 4. 1 Effective road plot obtained using envelope model on a step obstacle of height 1 cm

#### *Ramp Obstacle*

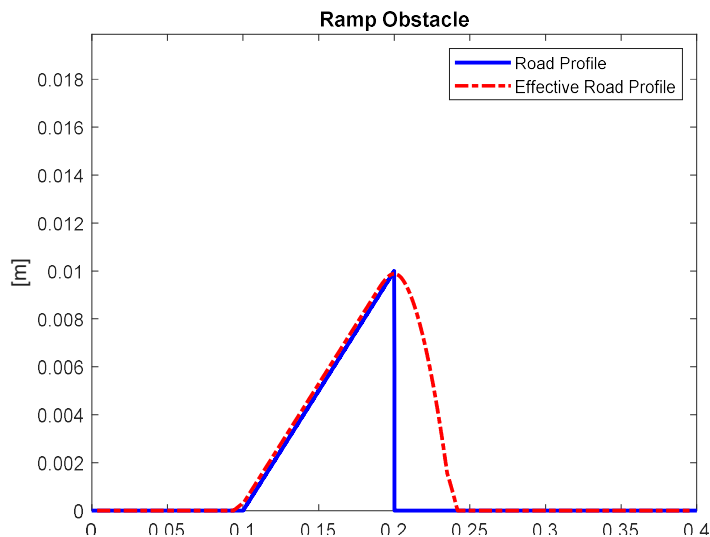


Figure 4. 2 Effective road plot obtained using envelope model on a ramp obstacle of height 1 cm

## Triangular obstacle

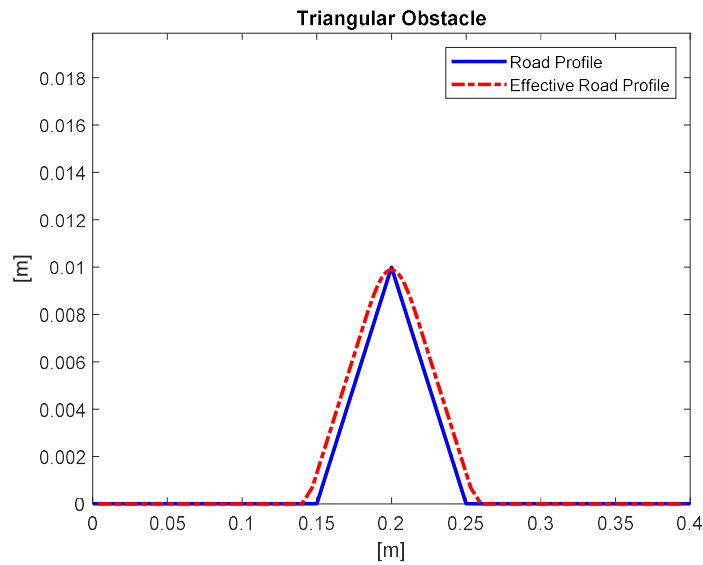


Figure 4. 3 Effective road plot obtained from envelope model on a triangular obstacle of height 1 cm

### 4.1.1 Sensitivity Analysis

In some cases an issue may arise, where the connecting rod at the bottom most points of the cams pierces the obstacle. Since the cams are supposed to represent the surface of the contact patch, this is not a physical phenomenon. To avoid this, one may increase the number of cams and take the average of their heights.

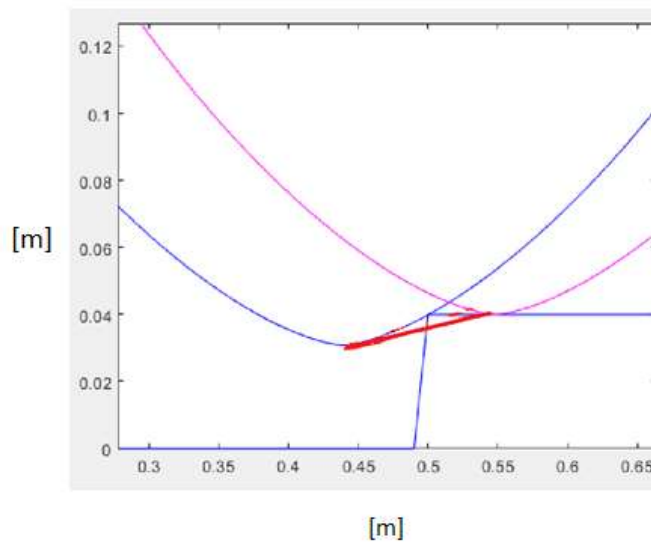


Figure 4. 4 Depiction of piercing of Contact patch surface by obstacle when model has insufficient number of cams

To understand the effects of increasing the number of cams on both the effective road profile, and the computational time required, a sensitivity analysis is performed. The various effective road profiles for a step obstacle of height 1 cm are plotted and the average time required for each test is recorded.

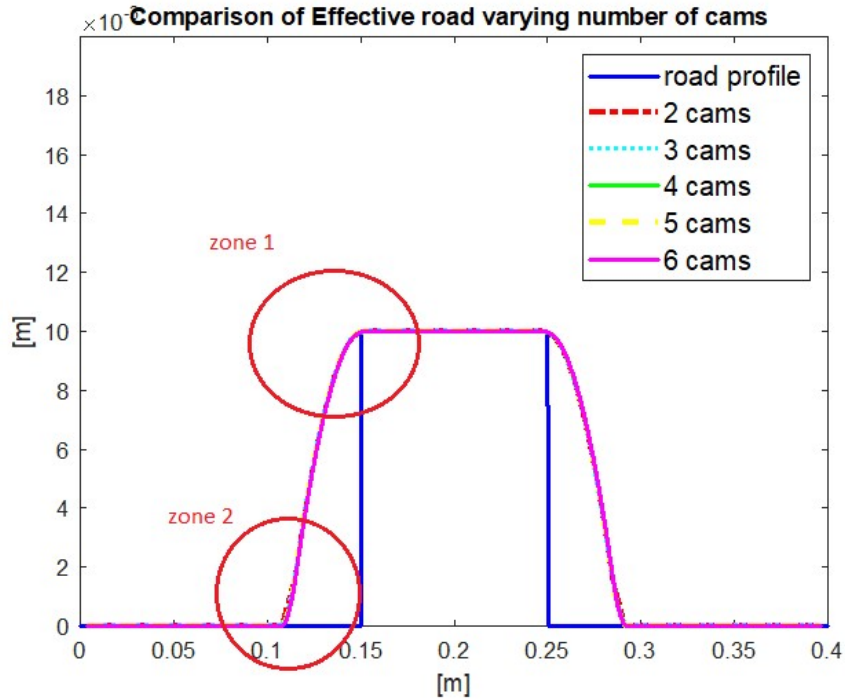


Figure 4.5 Comparison of envelope model results by varying the number of cams

To understand the variance in plot, zoomed in versions of zone 1 and 2 are as follows

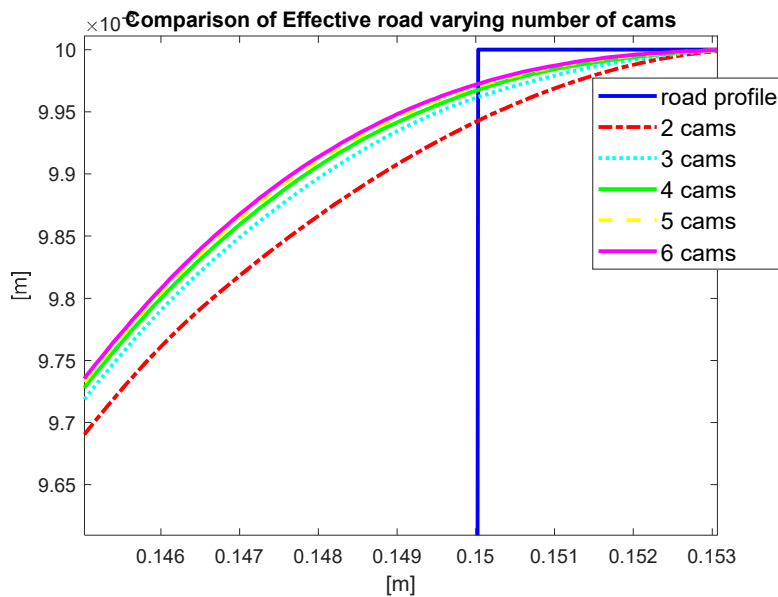


Figure 4.6 Zoomed in image of zone 1 in figure 4.5

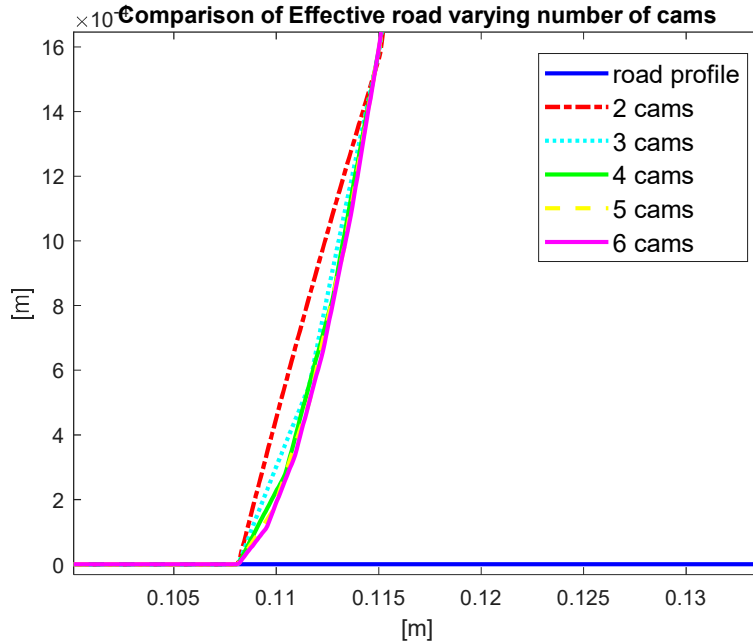


Figure 4. 7 Zoomed in image of zone 2 in figure 4.5

In both zones, it can be observed that from the 4<sup>th</sup> cam onwards , there isn't much difference in the plot of effective road with an increase in cams.

In order to determine the effect of the number of cams per unit length of the connecting rod, the same experiment may be repeated for increasing steps of connecting rod horizontal length  $l_s$ , and zone 1 can be compared.

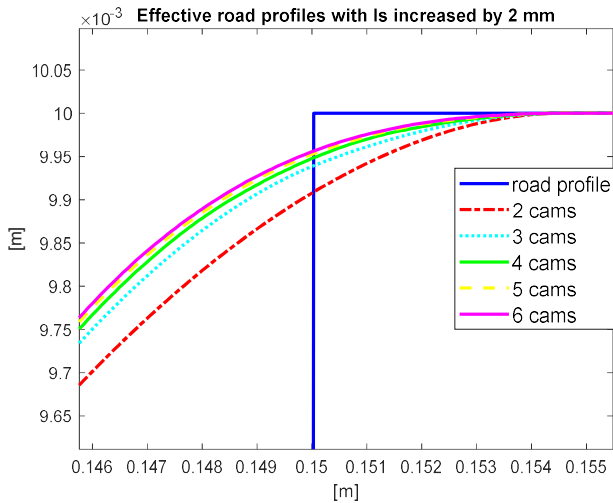


Figure 4. 9 Comparison of envelope model results for varying number of cams while  $l_s$  is increased by 2mm

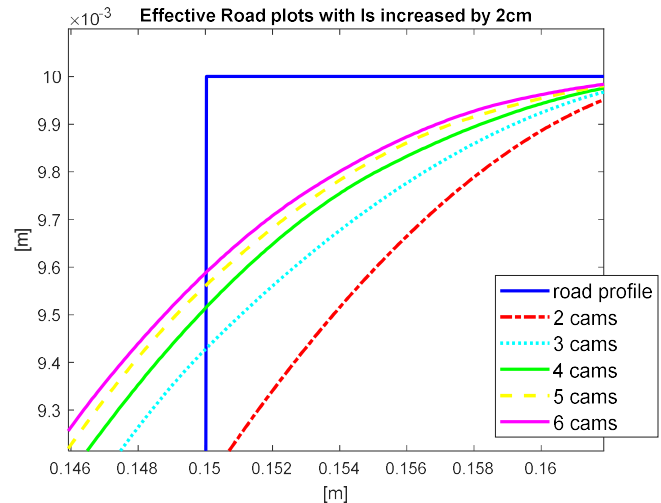


Figure 4. 8 Comparison of envelope model results for varying number of cams while  $l_s$  is increased by 2cm

It can be confirmed that as length of  $l_s$  increases, which is a result of the contact patch length increasing, the correspondence between 4 cam effective road and 5 cam effective road decreases, which implies it will take a higher number of cams for the resultant effective road plots to match closely. From this one can conclude that as the contact patch length increases, a higher number of cams may be utilized for a better approximation of the effective road profile.

The time required for computing the different number of cam models for an example step obstacle is given in the following table

*Table 5 Comparison of computational times for envelope models with increasing number of cams*

no. of cams	Simulation Time [s]	Increase in time wrt 2 cam
2	2.7879	
3	3.6875	32%
4	4.586	64%
5	5.3809	93%
6	6.2382	124%

## 4.2 Simulink Model

The aim of the final Simulink model is to solve the three equations (15),(16),(17) to obtain the vertical displacement, velocity and accelerations of the 3 degrees of freedom for every time instant for any given road profile. The model is the amalgamation of all the ideas and data derived till now.

Most of the data required to solve the equations are constants, either readily available e.g masses or calculated with simple equations e.g.  $k_b$ ,  $c_b$  . But two of the data required, namely the residual stiffness and the current height of the effective road are a bit more complex. This is a result of the dependence of the cam model properties on the tyre footprint, which is a function of the road reaction.

In the case of the residual stiffness a switch has to be implemented whereby if the effective road displacement is lower than that of the tyre, residual stiffness is made to be zero. In the alternative case, the value of the residual stiffness has to be obtained from a look up table with the data derived earlier where  $k_r$  is a function of the vertical displacement. The meaning of this switch is that when the tyre is not in contact with the road, the spring of stiffness  $k_r$  has to disappear, else it would wrongly act in the restorative direction, pulling the tyre towards the road, which is not a physical phenomenon.

In order to obtain the instantaneous height of the effective road, first the tyre footprint length is determined from the road reaction force which is calculated using the residual stiffness value supplied from the earlier function. Using the data where footprint length is plotted as a function of the vertical force, the corresponding tyre footprint length is obtained. This is supplied to a user defined matlab function that determines the cam properties of  $a_e$ ,  $b_e$ ,  $c_e$  and  $l_s$  . These values go to another function that determines the basicpath. The basicpath is the path a cam would traverse while going over the road profile. It is a necessary input to the instantaneous envelope model function that takes this data and the cam properties data to determine  $z_r$  , the effective road height at the given time instant.

### 4.2.1 Experiment and Results

The experiment is conducted by a rider on an e-scooter travelling at a constant velocity of 25 kmph over a known road profile. The road profile consists of 7 step obstacles of height 4mm.

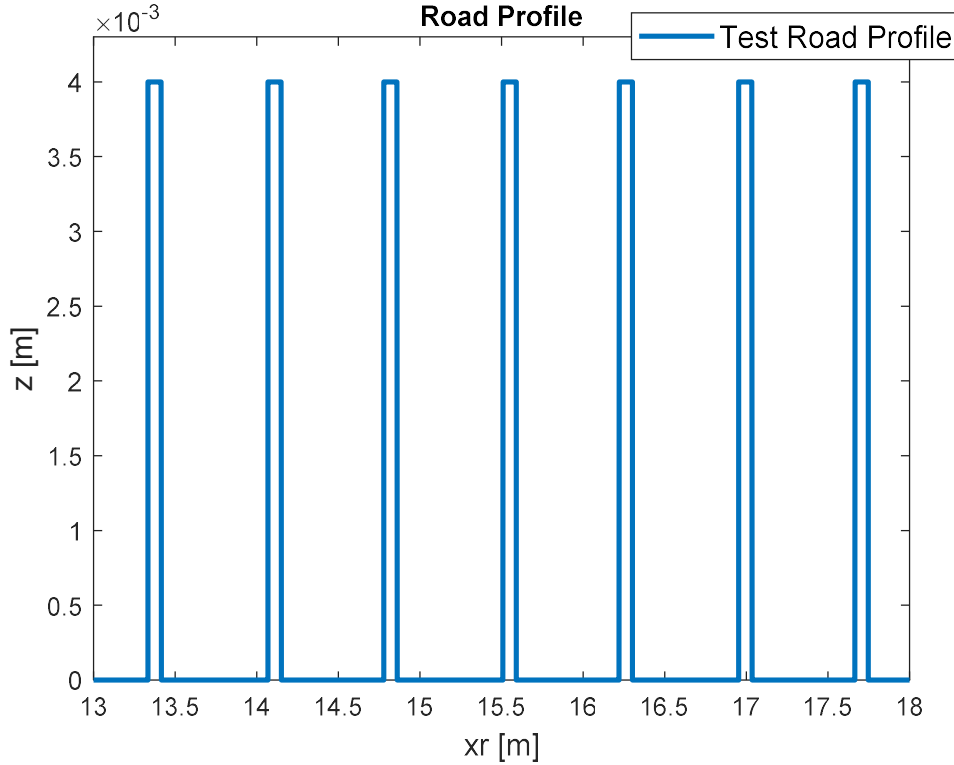


Figure 4. 10 Plot of the test road profile used in experiments

Sensors attached to the hub of the front and rear wheels capture the vertical acceleration. This data is compared with the model results.

The rider moving mass is a fraction of the original mass, denoted by  $m\_frac$ . The rider stiffness and damping  $k_h$  and  $c_h$ , along with  $m\_frac$  are tuned to match the experimental results with that of the model. Matlab Genetic Algorithm is used for this optimization process. The objective function is defined as the difference between avg values of peaks of the model data and experimental data. The optimization variables are set by defining a human body natural frequency range from 1 to 40 Hz, and damping factor range of 0.001 to 0.4. The stiffness can be calculated from

$$k_h = m_h w_n^2 \quad (24)$$

And damping coefficient from

$$c_h = 2\xi\sqrt{m_h k_h} \quad (25)$$

$M\_frac$  is given a range from 0.1 to 1.

The optimization variables are all scaled. The velocity of the tyre is reduced by 0.2 m/s in the model to match the peaks of the front wheel experimental results. The resultant values of  $k_h$  and  $c_h$ , along with  $m\_frac$  are used and the comparison of results for both front and rear wheels are as follows

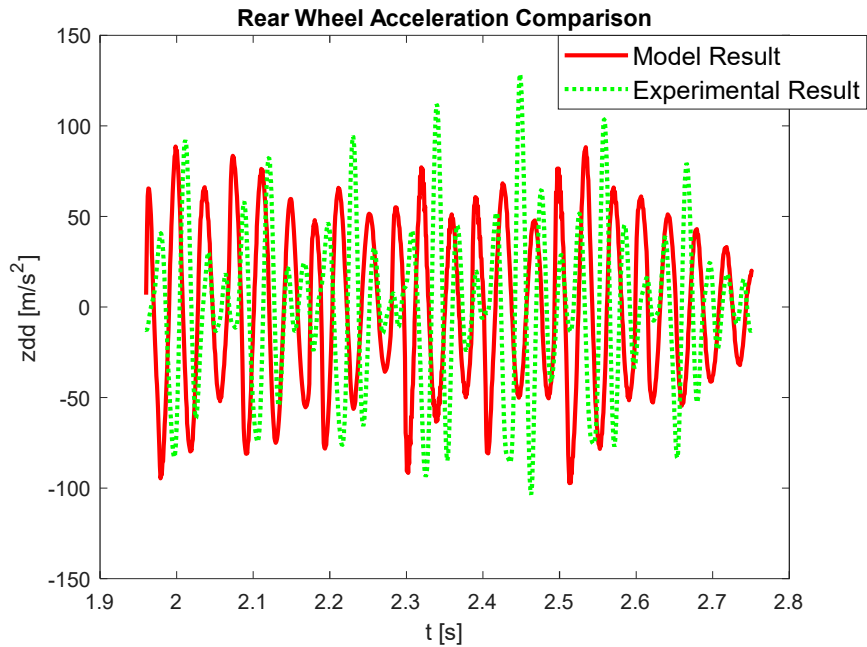


Figure 4. 11 Comparison of experimental and model results of Rear wheel acceleration

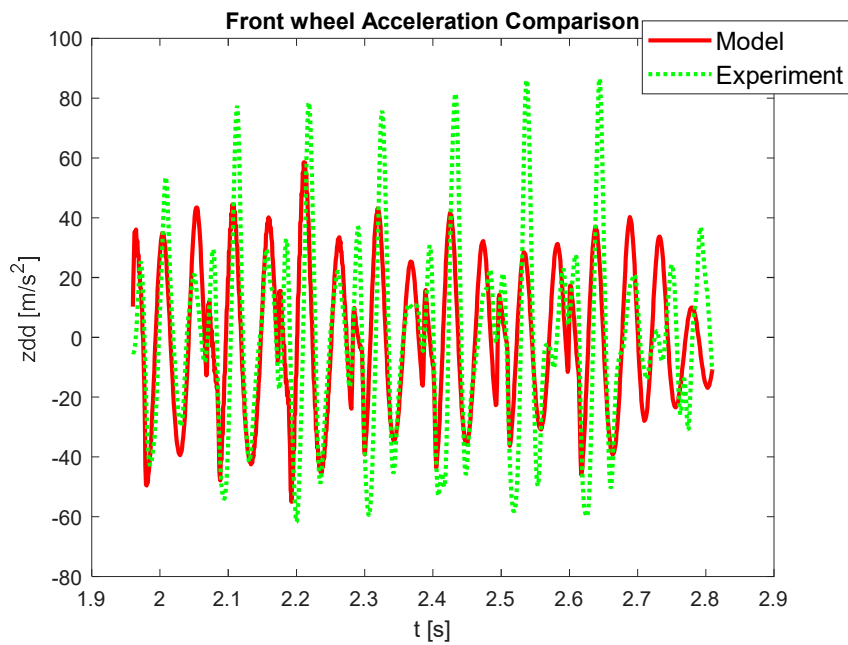


Figure 4. 12 Comparison of experimental and model results of Rear wheel acceleration

The variance seen in experimental results and model results may be attributed to the fact that a simplified model is used to evaluate the vertical dynamics.

# BIBLIOGRAPHY

- [1] A. J. C. Schmeitz, "A semi-empirical three-dimensional model of the pneumatic tyre rolling over arbitrarily uneven road surfaces," PhD Thesis, Delft University of Technology, Delft, 2004. Accessed: Mar. 06, 2025. [Online].
- [2] K. M. Captain, A. B. Boghani, and D. N. Wormley, "Analytical Tire Models for Dynamic Vehicle Simulation," *Vehicle System Dynamics*, vol. 8, no. 1, 1979, doi: 10.1080/00423117908968566.
- [3] J. M. Badalamenti and G. R. Doyle, "Radial-interradial spring tire models," *Journal of Vibration and Acoustics, Transactions of the ASME*, vol. 110, no. 1, 1988, doi: 10.1115/1.3269483.
- [4] P. W. A. , Zegelaar, "The dynamic response of tyres to brake torque variations and road unevennesses," 1998.
- [5] J. R. Kilner, "Pneumatic tire model for aircraft simulation," *J Aircr*, vol. 19, no. 10, 1982, doi: 10.2514/3.44786.
- [6] P. Bandel and C. Monguzzi, "SIMULATION MODEL OF THE DYNAMIC BEHAVIOR OF A TIRE RUNNING OVER AN OBSTACLE.," *Tire Sci Technol*, vol. 16, no. 2, 1988, doi: 10.2346/1.2148799.
- [7] A. J. C. Schmeitz and J. P. Pauwelussen, "An efficient dynamic ride and handling tyre model for arbitrary road unevennesses," in *Reifen, Fahrwerk, Fahrbahn: Tagung Hannover, 18-19 Oktober 2001*, VDI-Verlag, 2001, pp. 173–199.
- [8] A. J. C. Schmeitz and J. P. Pauwelussen, "High Frequency Tyre Response for Arbitrary Road Input," in *Veranstaltungsunterlagen Fahrwerktechnik, Haus der Technik, Tagung Nr. H030-06-23-0*, 2000.
- [9] M. Eichler, "A ride comfort tyre model for vibration analysis in full vehicle simulations," *Vehicle System Dynamics*, vol. 27, no. S1, pp. 109–122, 1997.
- [10] B. G. Kao and M. Muthukrishnan, "Tire transient analysis with an explicit finite element program," *Tire Sci Technol*, vol. 25, no. 4, pp. 230–244, 1997.
- [11] A. Kamoulakos and B. G. Kao, "Transient response of a rotating tire under multiple impacts with a road bump using PAM-SHOCK," in *Conference on High Performance Computing in Automotive Design, Engineering and Manufacturing*, 1996.

- [12] C. W. Mousseau, G. M. Hulbert, and S. K. Clark, "On the modeling of tires for the prediction of automotive durability loads," *Vehicle System Dynamics*, vol. 25, no. S1, pp. 466–488, 1996.
- [13] D. Belluzzo, F. Mancosu, R. Sangalli, F. Cheli, and S. Bruni, "New predictive model for the study of vertical forces (up to 250 Hz) induced on the tire hub by road irregularities," *Tire Sci Technol*, vol. 30, no. 1, pp. 2–18, 2002.
- [14] J. P. Maurice, "Short wavelength and dynamic tyre behaviour under lateral and combined slip conditions," *PhD thesis TU Delft*, 2000.
- [15] H. Shi and S. Maigengtian, "MF-Tyre MF-Swift 6.1.2 Equation Manual Three Dimensional Tyre Modeling Technique in Full Simulation Scenario. View project," 2010. [Online]. Available: <http://www.automotive.tno.nl>
- [16] A. J. C. Schmeitz, I. J. M. Besselink, and S. T. H. Jansen, "TNO MF-SWIFT," *Vehicle System Dynamics*, vol. 45, no. SUPPL. 1, pp. 121–137, 2007, doi: 10.1080/00423110701725208.
- [17] S. Chae, M. El-Gindy, M. Trivedi, I. Johansson, and F. O'ijer, "Dynamic response predictions of a truck tire using detailed finite element and rigid ring models," in *ASME International Mechanical Engineering Congress and Exposition*, 2004, pp. 861–871.
- [18] J. R. A. li and M. El-Gindy, "Advanced effective road profile filter for a rigid ring tyre quarter-vehicle model Advanced effective road profile filter for a rigid ring tyre quarter-vehicle model 29," 2013.